

Alma Mater Studiorum - Università di Bologna

FACOLTÀ DI SCIENZE MATEMATICHE, FISICHE E NATURALI

Corso di Laurea specialistica in Fisica

Dipartimento di Fisica

UNDULAR JUMP
NUMERICAL MODEL AND SENSITIVITY ANALYSIS

Tesi di laurea di:

MICHELE RAMAZZA

Relatore:

Prof. RAMBALDI SANDRO

Correlatori:

Prof. MANSERVISI SANDRO

Dott. CERVONE ANTONIO

Sessione III

Anno Accademico 2007-2008

CONTENTS

Abstract.....	5
Sommario.....	5
List of symbol	6
1.Introduction	8
1.1.Open channel flow.....	8
1.1.1.Introduction.....	8
1.1.2.Classification of open channel flows.....	8
1.1.3.Complexity	8
1.2.Bases of open channel hydraulics	10
1.2.1.Supercritical and subcritical flows.....	10
1.2.2.Momentum equation.....	11
1.2.3.Momentum function.....	11
1.2.4.Critical Flow	12
1.3.Hydraulic jump	12
1.3.1.Definition of hydraulic jump.....	12
1.3.2.Undular jump.....	13
1.3.3.Undular bore.....	14
1.3.4.Morning Glory.....	15
1.3.5.Two dimensional Approach.....	16
1.3.6.Momentum function balance.....	16
1.3.7.Undular surge, state of art	17
2.Open channel numerical modelling.....	18
2.1.Fluent.....	18
2.1.1.Introduction for open channel simulations with Fluent.....	18
2.1.2.User steps for open channel flow simulations	18
2.2.Generic fluid flow equations	19
2.2.1.Variables.....	19
2.2.2.Continuity and momentum equations	19
2.2.3.Transport equation discretization.....	19
2.2.4.Time evolution	20
2.2.5.Evaluation of gradients and derivatives	21
2.3.Volume of fluid, VOF.....	21
2.3.1.Overview	21
2.3.2.Geo-reconstruction method.....	21
2.4.Pressure based solver	22
2.4.1.Overview of pressure based solver.....	22
2.4.2.Discretization of continuity and momentum equations.....	22
2.4.3.Coupled solver	23
2.4.4.Multigrid method.....	23
2.5.Grid	23
2.6.Standard turbulence model.....	24
2.7.Wall functions	25
3.Undular jump simulation.....	27
3.1.Numerical modelling	27
3.1.1.Introduction to undular jump simulation.....	27
3.1.2.Operating conditions.....	27
3.1.3.Boundary: velocity inlet	28

3.1.4. Boundary: turbulent inlet quantities	28
3.1.5. Boundary: pressure outlet.....	29
3.1.6. Standard channel.....	29
3.2. Model validation	30
3.2.1. Grid sensitivity	30
3.2.2. Outlet sensitivity	33
3.2.3. Turbulent inlet sensitivity.....	33
3.2.4. Undular jump experiment	36
3.2.5. Free surface data comparison	37
3.3. Undular jump fields.....	38
3.3.1. Velocity fields	38
3.3.2. Static pressure profiles.....	38
3.3.3. Vorticity field.....	40
3.4. Undular jump sensitivity analysis.....	41
3.4.1. Velocity inlet profile	41
3.4.2. Turbulent kinetic energy	44
3.4.3. Froude number	45
3.4.4. Instability for critical waves.....	49
4. Conclusions.....	51
4.1. Undular jump	51
4.1.1. General considerations.....	51
4.1.2. Necessary parametrized models.....	51
4.1.3. Sensitivity.....	52
4.1.4. Essential physical conditions.....	52
4.1.5. Wave characteristic, dependencies from Froude number.....	52
4.2. Applicability of the model to open channel studies.....	53
4.2.1. Applicability fields.....	53
4.2.2. Computation cost	53
4.3. Future studies	54
4.3.1. Improving the model	54
4.3.2. Possible applications	54
Appendix A.....	57
Appendix B.....	57
References.....	59

Abstract

The open channel flow is the object of this work which aims to study near-critical flows through numerical simulations. As first step, the problem of the undular hydraulic jump is defined and the basic open channel equations are introduced. We use the near-critical flow of the undular jump to validate the numerical model. The numerical simulations are performed by using the commercial code Fluent with VOF multiphase model, pressure based explicit solver, geometric interface reconstruction and standard $k-\epsilon$ turbulence model. Options and specific details of the model are presented in the corresponding sections. The model shows that wide open-channel flows can be studied with two dimensional grids. In this work we also report simulations and the sensitivity analysis of the undular jump to better understand this phenomenon. Inflow organization in a vertical shear seems to be a necessary condition to create a detachment of the boundary layer that necessarily has to occur in the undular jump. As a possible application, this model can be used to better understand wave formation mechanism and, with a three dimensional implementation, design near-critical open channel for recreational use. Computational cost are examined in the conclusions because it must to be considered for large or three dimensional domains.

Sommario

I flussi quasi-critici nei canali a superficie libera possono essere studiati con simulazioni numeriche. Nella parte introduttiva del presente lavoro si definisce il problema del “undular hydraulic jump” riassumendo le equazioni di base per i canali a superficie libera. Il “undular hydraulic jump” viene utilizzato come fenomeno di riferimento per la validazione del modello numerico implementato attraverso il codice commerciale Fluent. Tale codice è basato su un solutore accoppiato, contenente modelli multifase a volume di fluido, con ricostruzione geometrica dell'interfaccia e con un modello di turbolenza standard $k-\epsilon$. Tutti i modelli e le equazioni utilizzate sono specificati in un capitolo dedicato. Le simulazioni effettuate mostrano che i flussi a superficie libera in canali con sezione regolare possono essere studiati con modelli bidimensionali. Sono state inoltre effettuate analisi di sensitività delle condizioni al contorno. L'organizzazione del profilo verticale delle velocità del flusso entrante sembra essere un fattore determinante per il distacco del “boundary layer” e conseguente creazione di onde senza frangimento. Il modello può essere utilizzato per comprendere meglio il meccanismo di formazione delle onde in presenza di geometrie più complicate e, con una implementazione tridimensionale, per progettare canali a scopo ricreativo. I costi computazionali sono esaminati nelle conclusioni in quanto sono un parametro significativo per la realizzabilità di tali applicazioni.

List of symbol

A	= cross sectional area normal to the channel bottom (m^2)
V	= average velocity of the flow (m/s)
P	= wet perimeter length
$Q=VA$	= discharge ($\text{m}^3 \text{s}^{-1}$)
$\vec{u} \vec{v}$	= velocity vector (m/s)
$q=Vy$	= two dimensional discharge ($\text{m}^2 \text{s}^{-1}$)
T	= width at the top of the free surface (m)
D	= hydraulic depth (m)
D_h	= hydraulic radius
y	= flow depth measured perpendicular to the channel bottom (m)
Fr	= Froude number
Re	= Reynolds number
y_c	= critical flow depth (m)
y_{fs}	= free surface height (m)
S	= wave steepness (x-y ratio)
b	= channel width in a rectangular section (m)
a_w	= wave amplitude from first crest to first trough
δ	= grid point per characteristic length
F	= momentum function
I	= turbulent intensity
l	= turbulent length scale
L_i	= generic length scale for the i^{th} dimension
L_w	= wavelength
k	= turbulent kinetic energy

ϵ	= turbulent dissipation rate
N	= exponent in the velocity profile
g	= gravity constant: 9.81 (m s ⁻²)
ρ	= density (water: 998 kg/m ³)
μ	= dynamic viscosity (1.002 10 ⁻³ N s m ⁻²)
ν	= kinematic viscosity (1.004 10 ⁻⁶ m ² s ⁻¹)
ρ_0	= operating density (air: 1.223 kg/m ³)
p	= total static pressure (Pa)
p_0	= reference (atmospheric) pressure (101325 Pa)
α	= volume fraction
$\bar{\tau}$	= stress tensor
J_f	= face flux

1. Introduction

1.1. Open channel flow

1.1.1. Introduction

Open channels are fluid flows under gravitational force with the free surface forced only by atmospheric pressure. This makes the study of this flow more complicated than the pipe flow in which simpler boundary conditions can be applied. In open channels, the free surface is an unknown field a priori. The flow depth, the discharge, the slope of channel bottom and the free surface are independent fields. Natural rivers and artificial channels can show non regular section and roughness. In general, the treatment of open channel flow is something more empirical than of pipes [35].

1.1.2. Classification of open channel flows

At first, we can classify the flow with free surface in *steady* and *unsteady*, knowing that the treatment of unsteady flows is really much more complicated and moreover, some basic quantities as discharge, momentum and energy are not conserved along the channel. Steady flows can be treated using discharge and energy conservation. Rivers without flooding effects and relatively quiet can be considered steady flows in the average quantities. Turbulent effects can be treated as random processes if their scales are smaller than the average flow scale. Higher energy flows can show turbulent effect on the same scale of the flow, but it will not be treated in this work. A second classification of channel flows can regard their variability in the space. When the flow maintains all its characteristics along the course is called a *uniform flow*. This regime is common in artificial channels. If the space variability becomes important, but still gradual, we have the *gradually varied flow*. An example can be a channel that slowly changes its steepness. When the flow depth changes abruptly with the space we have a *rapidly varied flow* [35]. Steady and rapidly varied flows are the subject of this study. Turbulent level of an open channel is classified with the Reynolds number:

$$Re = \frac{V D_h}{\nu} \quad (1-1)$$
$$D_h = \frac{4A}{P}$$

where D_h is the hydraulic radius, A is the cross-sectional area and P is the wet perimeter. The value of Re in the present study flow is about 10^5 .

1.1.3. Complexity

In rivers or artificial channels where rapidly varied flow occurs, it's possible to observe steady three-dimensional organized structures. These structures are common to all the rivers and show scale invariance. The free surface shape and the back flows with air entrainment, known as foam or white water, characterize these waves, rollers, drops, shock waves, etc. People use this water structures for recreational sports like kayaking, rafting and river boarding (Fig 1-1, Fig 1-2) and they know, or they should know, all the dangerous consequences associated with these structures. Kayakers and rafters can

spend years and years riding different rivers all over the world trying to understand water organization in order to be able to predict the effects on the boat. The author has developed this experience in several year of kayaking and rafting practice. A description of similar structures is presented in hydraulic books because they must be taken into account in the design of hydraulic works. Thus, most part of the knowledge about water structures is oriented on the design of dams, hydraulic drops and all sort of artificial works. These works however, usually study channel flows really different from natural rivers flows. River beds present many types of irregular rocks, from big boulder to small rocks while concrete works are smooth and regular with geometrical shapes. In general, artificial flows in hydraulic works are forced by the geometry and far from the critical state (see 1.2.4.). This means that in general more energy is involved, yielding strong behaviors of the flows. In natural rivers instead the water erosion and the rumbling rock carried downstream by the flow, design the river bed through the time. Depending on the average steepness, the result is a wavy flow usually close to the critical state. In general, given a river bed, it's almost impossible to predict the stationary flow with a sufficient precision to resolve water structures while in geometric works the studies are easier. Only few simple cases of near-critical flow in simple channels have been studied and a prediction of the flow in terms of free surface, velocity field, etc. has been done. Even in these cases, laboratory experiments are necessary to confirm these studies. Natural rivers with rocky bed are characterized by strong roughness and a great amount of energy is dissipated by turbulent roller and friction thus, an analytical treatment of a complex river flow could results really hard or impossible. For these reasons a complex system approach to pinpoint the emergent structures and the critical transitional parameters is suggested to better understand water organization in natural rivers. Complexity can be studied with numerical simulations and this work is a step in this direction. Later on it will be showed a discussion of the undular jump, a water structure well known in hydraulic. On the undular jump we test our numerical model and perform some sensitivity analysis.



Fig 1-1: Kayakers surfing a natural roller in Uganda, White Nile.



Fig 1-2: hydraulic jump in the natural Raundalselva river, Norway (photo by the author)

1.2. Bases of open channel hydraulics

1.2.1. Supercritical and subcritical flows

In open channel flows, the effect of gravity upon the state of the flow is represented by a ratio of inertial forces to gravity forces. This ratio is given by the *Froude number*, defined as

$$Fr = \frac{V}{\sqrt{gD}} \quad (1-2)$$

where V is the mean velocity of the flow, g is the gravity acceleration, D the hydraulic depth. All the quantities are defined in the “List of symbol “ pg 6. If Fr is equal to unit, the flow is said to be in the *critical state*. For such condition, Eq.(1-2) gives

$$V = \sqrt{gD} \quad (1-3)$$

In critical state the mean velocity of the flow is equal to the shallow water gravity waves velocity. If $Fr < 1$ the flow is called *subcritical*; the role played by inertial forces is less pronounced and the flow is defined as tranquil and streaming. If $Fr > 1$ the flow is called *supercritical*; the role played by inertial forces is more pronounced and is characterized by high velocity and defined as rapid and torrential [35]. It is also possible to define the subcritical flow as the flow controlled by the downstream condition, instead, the supercritical flow is controlled by the upstream condition. This means signal or information can be carried upstream only in case of subcritical flow.

1.2.2. Momentum equation

The momentum of the flow per unit time passing a channel section is expressed by

$$\beta Q \rho V \quad (1-4)$$

where β is the momentum coefficient for the non uniform velocity

$$\beta = \frac{\int_A v^2 dA}{V^2 A} \quad (1-5)$$

Q the discharge, ρ the density of the water and V the mean velocity in the channel section [35]. According to Newton's second law of motion, the change of momentum per unit time in the body of water between two section 1 and 2 may be written as:

$$Q \rho (\beta_2 V_2 - \beta_1 V_1) = P_1 - P_2 + W \sin(\theta) - F_f \quad (1-6)$$

where P are the pressure acting on the section and W is the weigh of the water between the two section and F_f is the total friction force acting along the surface of the channel. Assuming hydrostatic pressure

$$P_i = b \int_0^{y_i} \rho g y_i dy = b \frac{1}{2} \rho g y_i^2 \quad (1-7)$$

and

$$\begin{aligned} W &= \rho g (\bar{y} b L) \\ \sin(\theta) &= \frac{z_1 - z_2}{L} \end{aligned} \quad (1-8)$$

where b is the channel width and L the distance between the two sections, we can simplify the (1-6) having

$$z_1 + y_1 + \beta_1 \frac{V_1^2}{2g} = z_2 + y_2 + \beta_2 \frac{V_2^2}{2g} + h_f \quad (1-9)$$

The friction term h_f measure the losses due to external forces (channel bed) exerted on the water by the walls of the channel. [35]

1.2.3. Momentum function

In applying Eq.(1-9) in a short horizontal reach of a prismatic channel, the external force of friction and the weight effect of the water can be ignored. Thus, with $\theta=0$ and $F_f=0$ Eq.(1-6) becomes

$$Q \rho (\beta_2 V_2 - \beta_1 V_1) = P_1 - P_2 \quad (1-10)$$

Assuming Eq.(1-7) we have

$$\rho \beta_2 \frac{Q^2}{A_2} + \frac{1}{2} \rho g A_2 y_2 = \rho \beta_1 \frac{Q^2}{A_1} + \frac{1}{2} \rho g A_1 y_1 \quad (1-11)$$

$$\beta_2 \frac{Q^2}{g A_2} + A_2 \frac{y_2}{2} = \beta_1 \frac{Q^2}{g A_1} + A_1 \frac{y_1}{2}$$

Eq.(1-11) show a conservation quantity which is defined as *momentum function*

$$F = \beta \frac{Q^2}{g A} + A \frac{y}{2} \quad (1-12)$$

The first term is the momentum of the flow passing through the channel section per unit time per unit weight, and the second is the force per unit weight. Both terms are essentially force per unit weight. Neglecting friction, in steady flows, momentum function have to be conserved along the channel [35].

1.2.4. Critical Flow

The critical state of flow is defined as the condition for which the Froude number is equal to unity. Thus, the velocity of the flow is equal to the velocity of the shallow water waves. This state splits the subcritical and the supercritical flow range. The critical flow depth in a horizontal channel is therefore

$$y_c = \frac{V^2}{g} \quad (1-13)$$

A more common definition is when the specific energy have a minimum for a given discharge [32].

1.3. Hydraulic jump

1.3.1. Definition of hydraulic jump

The hydraulic jump in open channel occurs when the flow turn from supercritical to subcritical regime. The flow depth change rapidly from a low stage to an high stage. The result is usually an abrupt rise of water surface [35]. This local phenomenon is known as *hydraulic jump*. When the jump is high, that is, when the change in depth is great, the jump is called *direct jump*. The direct jump involve a large amount of energy loss through dissipation in the turbulent body of water in the jump. Consequently, the energy content in the flow after the jump is appreciably less than before. This phenomenon occur also in the house sink when the rapid flow turns into a thicker flow (Fig 1-3). The wall of the sink create a sort of dam that slow down the water creating a subcritical flow region.



Fig 1-3: Direct jump in the house sink

1.3.2. Undular jump

An hydraulic jump with a small change in depth is called an *undular jump*. This flow regime is referred to as near critical flow. The water doesn't rise abruptly but passes through stationary undulation of the free surface gradually diminishing in size. The energy is not dissipated locally but is radiated downstream with the wave train and gradually lost due to turbulent dissipation effects. The undular jump is a quite common phenomenon in the natural rivers where flow can turn many times from supercritical to subcritical. Generally, due to the non-symmetry of the river bed, waves don't look always very smooth and regular. Sometimes, generally in artificial channels or rivers with a smooth bed rock, it is possible to observe undular jump with a lot of regular waves downstream the jump (Fig 1-4). The waves generated by the jump are stationary in a first section after the jump. Laboratory experiments, where the wave train is free to propagate downstream, indicate an organized region with stationary waves in a number of wave lengths between 3 and 10 depending on the Froude number. Downstream of the organized region, the free-surface exhibits a chaotic, unsteady pattern where no visible periodicity is visible [23]. Further downstream a damping flow region exists where wave amplitude tends to zero and all jump energy is completely lost.



Fig 1-4: Natural undular jump. Vosso river; Voss, Norway

1.3.3. Undular bore

A similar phenomenon may occur in estuaries funnel shaped with a large tidal range (Fig 1-5). This characteristic event is define as a *hydraulic jump in translation* [24]. This event is well known from shipping companies because has been the reason of several boat sinking in rivers close to the sea. It's also appreciate from surfers because they like very smooth and long waves. The waves or the roll formed at the front have an upstream traveling velocity. Similar equations are valid for both, traveling and stationary, undular jump with care on the definition of the reference system. This wave is a case of unsteady flow but can be treated as steady in a mobile reference system considering the quasi-constant speed of the tidal bore. Undular bore is probably the simplest phenomenon of positive undular surge because of the absence of inflow turbulence. For this reason analytical equations can be applied to study this phenomenon if the free surface has a solid aspect [10].



Fig 1-5: tidal bore of the Dordogne river in Sept. 2006 (Courtesy of Antony Colas) – bore propagation from left to right.

1.3.4. Morning Glory

In the atmosphere, a phenomenon called “*Morning glory*” may occur in few places in the world and the formation mechanism has been compared with the hydraulic jump by Clarke [15]. The clouds formed in these condition are very spectacular and are a pilot attraction (Fig 1-6). Theirs formation should be favored by a slight synoptic pressure gradient, cloudless sky, shallow chilled layer descending a steep and smooth hill at low latitude. The cold air, cooled by night effect, run down the hill with a steep pressure gradient at the front, this flow act like a tidal bore in a river forming a wave train of clouds or a single turbulent cloud at the front.



Fig 1-6: Morning glory clouds over the gulf of Carpentaria, Australia. 2001 (www.dropbears.com)

1.3.5. Two dimensional Approach

Observations in the central region of wide open channel show that the flow properties are essentially the same of a rectangular channel of infinite width. This region exists in regular channels only when the width is greater than 5 to 10 times the depth of the flow depending on the surface roughness of the side walls [35]. Thus, far from the wall and in straight regular channel, we can treat the flow as two dimensional. Perpendicular velocity fluctuation can be taken in account in turbulence model. All flow properties are expected to be conserved along the width of the channel in the central area. It's possible to define all open channel hydraulic quantities for unit width for the two dimensional case, for example:

$$Q = VA \rightarrow \frac{Q}{b} = q = Vy$$

$$F = \beta \frac{Q^2}{gA} + A \frac{y}{2} \rightarrow \frac{F}{b} = f = \beta \frac{V^2 y}{g} + \frac{y^2}{2}$$

For simplicity, this approach will be imply in evident two dimensional study and small letter will be used to indicate related quantities. For numerical studies this approach reduces evidently the calculation cost. Three dimensional turbulence can be treated in a numerical two dimensional approach because models try to parametrize all the turbulent effects. Hydraulic jumps and undular bores can be treated as two dimensional in wide open channel in which side effects and shock waves are confined close to the bank and they do not interfere with the central flow (Fig 1-5 and Fig 1-4 show cases in which a two dimensional approach is appropriate).

1.3.6. Momentum function balance

In hydraulic jumps in an horizontal channels, momentum function have to be the same before and after the jump because of the momentum equation. The flow depth before the jump is called *initial depth* and after the jump *sequent depth* respectively y_1 and y_2 (Fig 1-7). Momentum function equation became

$$\beta_1 V_1^2 \frac{A_1}{g} + \frac{y_1^2}{2} b = \beta_2 V_2^2 \frac{A_2}{g} + \frac{y_2^2}{2} b \quad (1-14)$$

With some algebra, using some basic equation (see details in Appendix A p.57) and considering coefficient $\beta_1 = \beta_2 = \beta$ we have a relation between the initial depth and the sequent depth.

$$\frac{y_2}{y_1} = \frac{1}{2} \left(\sqrt{1 + 8\beta F_1^2} - 1 \right) \quad (1-15)$$

This equation can be considered a necessary condition for the hydraulic jump formation. The relation between y_1 and y_2 is driven by the upstream Froude number, it's therefore considered as a driving parameter because define adimensionally the flow. For small Froude number undular jump with smooth oscillating surface is observed. Experiments show that the disappearance of free-surface undulation and the formation of roller take place in a range from 1.5 to 4 [22] depending on the aspect ratio and on three dimensional effects. Increasing F_1 it's possible to assist to a wave breaking and the flow form a *roll* which is characterized by an air entrainment and backward flow at the top of the free surface (Fig 1-2 show a broken wave with a roll on

river right). Authors give different threshold for the roll formation because we will see that many parameters are involved in the determination of the wave amplitude.

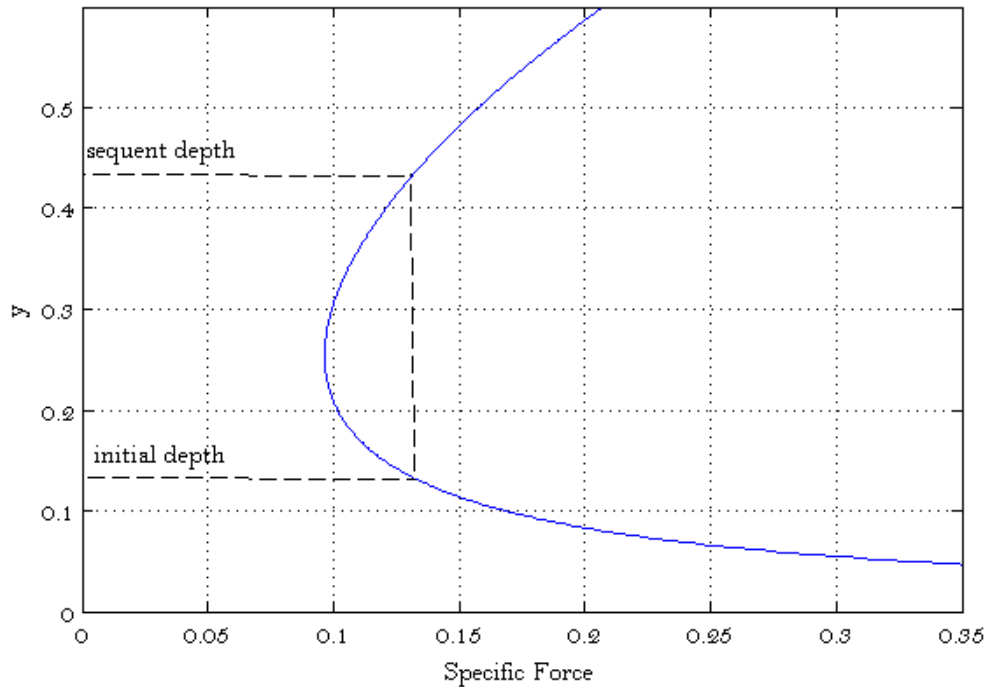


Fig 1-7: Momentum function plotted against flow depth in a two dimensional channel. Inflow Froude number = 1.4 and $q = 0.4 \text{ m}^2/\text{s}$

1.3.7. Undular surge, state of art

One of the classic paper on the undular jump is Montes (1986) [28]. A recent review of the state of art is presented by Chanson [22] and reported here. Chanson present also results from experiments and new considerations about the analogy between stationary and translational undular jump. Analytical theory of the hydraulic jump has been studied by Boussinesq [27] and Montes [30]. Important experiment and studies about undular jump classification in non-wide channel have been performed and well detailed by Chanson [23]. Positive surge were studied by hydraulicians and applied mathematicians for a few centuries. Major contributions included the works of Barré de Saint-Venant [3], Boussinesq [31], and more recently Lemoine [33], Serre [17] and Benjamin and Lighthill [16]. Several researchers discussed the development of a positive surge [14][2]. Classical experimental investigations of undular surges include Darcy and Bazin [26], Favre [25], Zienkiewicz and Sandover [11], Sandover and Holmes [9], Benet and Cunge [4]. Ponsy and Carbonnell [6] and Treske [1] presented a comprehensive description of positive surges in trapezoidal channels of large sizes. Pertinent reviews comprised Benjamin and Lighthill [34], Sander and Hutter [7] and Cunge [8]. Recent numerical studies encompassed Madsen and Svendsen [13] on the stationary jump, and Caputo and Stepanyants [10], Madsen et al. [12] and El et al. [5] on advancing bores. Recent studies of undular tidal bore (Chanson [24]) show results of a simple undular jump experiment in order to model the undular bore.

2. Open channel numerical modelling

2.1. *Fluent*

2.1.1. Introduction for open channel simulations with Fluent

Fluent is a commercial general purpose fluid dynamics simulator. The 6.3 two-dimensional version is used in all simulations. Grid domain can be generated by a specific program called Gambit. Fluent accepts unstructured grid and, if necessary, this feature permits easy refinement of the region of interest. Fluent provides a multiphase model called *VOF* (Volume Of Fluid) allowing multiple phases modeling. Thus it can simulate open channel flows using two fluids: air and water. Open channel options are available with VOF to model specific condition as constant atmospheric pressure for the air, special outflow boundary and interface reconstruction. Fluent works with mean value in each cell center and uses turbulence model to simulate non laminar effects. With Fluent all kinds of post processing are possible and data can be exported easily. Although Fluent can use solver schemes to reach convergence, numerical stability is not guaranteed and care is necessary in defining the time step, the grid resolution and the initial condition. A review of all models used in the simulation will be given in next paragraphs. More details are available on Fluent user guide manual [18] and Gambit manual.

2.1.2. User steps for open channel flow simulations

Fluent, like every numerical simulator, requires few steps to define the problem, the model to be used, and all numerical parameters. The steps can be summarized as follows:

In Gambit

- Definition of the geometry and the mesh
- Definition of the boundary

In Fluent

- Import the mesh
- Definition of models and solver parameters
- Definition of boundary conditions and operating conditions
- Initialize the solver with arbitrary initial conditions
- Iterate solver algorithm
- Check the stability of the iterations and save the results.

Paragraph 3.1. shows detailed options of the model used and paragraph 2.4. shows the solver properties.

2.2. Generic fluid flow equations

2.2.1. Variables

Fluent stores all the necessary variables in the center position of the cells. In two dimensional open channel the necessary variables are

u, v fluid velocity

α volume fraction

p pressure

k, ϵ turbulent kinetic energy and dissipation rate (for a $k-\epsilon$ model)

2.2.2. Continuity and momentum equations

For all flows, Fluent solves conservation equations for mass and momentum. The equation for conservation of mass, or continuity equation, can be written as follows

$$\nabla \cdot \vec{v} = 0 \quad (2-1)$$

Conservation of momentum in a inertial reference frame is described by [19].

$$\frac{\partial}{\partial t}(\rho \vec{v}) + \nabla \cdot (\rho \vec{v} \vec{v}) = -\nabla p + \nabla \cdot (\bar{\bar{\tau}}) + \rho \vec{g} \quad (2-2)$$

where $\bar{\bar{\tau}}$ is the stress tensor

$$\bar{\bar{\tau}} = \mu [(\nabla \vec{v} + \nabla \vec{v}^T)] \quad (2-3)$$

2.2.3. Transport equation discretization

Fluent uses a control-volume-based technique to convert a general scalar transport equation to an algebraic equation that can be solved numerically. This control volume technique consists of integrating the transport equation about each control volume Eq. (2-4), yielding a discrete equation that expresses the conservation law on a control-volume basis. Discretization of the governing equations can be illustrated considering the unsteady conservation equation for transport of a general scalar quantity ϕ :

$$\int_V \frac{\partial \rho \phi}{\partial t} dV + \oint \rho \phi \vec{v} \cdot d\vec{A} = \oint \Gamma_\phi \nabla \phi \cdot d\vec{A} + \int_V S_\phi dV \quad (2-4)$$

where

ρ = density

\vec{v} = velocity vector

\vec{A} = surface area vector

Γ_ϕ = diffusion coefficient for ϕ

S_ϕ = sources and sinks of ϕ per unit volume

Discretization of Eq. (2-4) is presented in Eq.(2-5) where the value of ϕ is placed in the cell center and the value at the volume boundary faces ϕ_f is calculated using an

interpolation first-order upwind scheme

$$\frac{\partial \rho \phi}{\partial t} V + \sum_f^{N_{faces}} \rho_f \vec{v}_f \phi_f \cdot \vec{A}_f = \sum_f^{N_{faces}} \Gamma_\phi \nabla \phi_f \cdot \vec{A}_f + S_\phi V \quad (2-5)$$

where

N_{faces} = number of faces enclosing cell

V = cell volume

This numerical discretization is not used for the VOF equation. VOF model uses a more accurate scheme in order to simulate discontinuous fields like the color function which defines the interface between two different fluids (see 2.3.2.).

This equation contains the unknown scalar variable at the cell center as well as the unknown values in surrounding neighbor cells. Thus, Eq. (2-5) will be in general non-linear. A linearized form must be used with algebraic linear solvers and therefore one must solve the above discrete equation in the following linear form

$$a_p \phi = \sum_f a_{nb} \phi_{nb} + b \quad (2-6)$$

where the subscript nb refers to neighbor cells and a_p and a_{nb} are the linearized coefficients for ϕ and ϕ_{nb} . b represents the source term. Similar equations can be written for each cell in the grid yielding a set of algebraic equations with a sparse coefficient matrix. For scalar equations Fluent solves this linear system using a point implicit (Gauss-Seidel) linear equation solver in conjunction with an algebraic multigrid method (see 2.4.4.).

2.2.4. Time evolution

A generic expression for the time evolution of a general variable ϕ is given by

$$\frac{\partial \phi}{\partial t} = F(\phi) \quad (2-7)$$

where the F function incorporate all spatial terms. A first order discretization is given by the *implicit time integration*

$$\begin{aligned} \frac{\phi^{n+1} - \phi^n}{\Delta t} &= F(\phi^{n+1}) \\ \phi^{n+1} &= \phi^n + \Delta t F(\phi^{n+1}) \end{aligned} \quad (2-8)$$

which yields the equation for the time evolution of the quantities in Eq. (2-8 b). This scheme is called *implicit* since the unknown ϕ^{n+1} at the time $n+1$ in a given cell is related through $F(\phi^{n+1})$ which is a function of ϕ^{n+1} itself. This equation can be solved iteratively at each time before moving to the next step. The advantage of this scheme is that it is unconditionally stable with respect to time step size. This process can be controlled by the *solver* in several ways which are described in paragraph 2.4..

2.2.5. Evaluation of gradients and derivatives

Gradients are needed not only for constructing values of a scalar at the cell faces, but also for computing secondary diffusion terms and velocity derivatives. The gradient $\nabla \phi$ of a given variable ϕ is used to discretize the convection and diffusion terms in the conservation equations Eq.(2-1) and (2-2). Gradient is computed according to *Green-Gauss Cell-Based* methods. The value of the gradient of a general quantity in the cell center $\nabla \phi_{c0}$ is calculated numerically by

$$(\nabla \phi)_{c0} = \frac{1}{\nu} \sum_f \bar{\phi}_f \vec{A}_f \quad (2-9)$$

where the face value, $\bar{\phi}_f$, is taken from the arithmetic average of the values at the neighboring cell centers and ν is a coefficient.

2.3. Volume of fluid, VOF

2.3.1. Overview

VOF model introduces a variable containing the volume fraction of each phase; the sum of all fractions has to be 1. The fields for all variables and properties are shared by the phases and represent volume-averaged values, as soon as the volume fraction of each phase is known at each location. For open channel simulations a very small number of cells are expected to have both phases at the same time if no air entrainment is occurring. This approach permits the simulation of open channels in which the geometry of the water flow is unknown a priori and atmospheric pressure is maintained at the free surface. Fluent simulates both air and water motions in a wall bounded channel. This is not strictly correct because the open channel atmosphere is not confined. Effects of the upper boundary are however negligible because the air motion has weak interaction with water flow. VOF model solves continuity equations with the phase variable for the q -th phase:

$$\frac{\partial \alpha_q \rho_q}{\partial t} + \nabla \cdot (\alpha_q \rho_q \vec{v}) = 0 \quad (2-10)$$

Since mass transfer between the phases in open channel can be ignored, the right hand side of Eq. (2-10) doesn't have any source terms.

2.3.2. Geo-reconstruction method

In the geometric reconstruction approach, standard interpolation schemes are used to obtain the face fluxes whenever a cell is completely filled with one phase or another. When the cell contains both phases, the geometric reconstruction scheme is used. The geometric reconstruction scheme describes the interface between fluids using a piecewise-linear approach. It assumes that the interface between two fluids has a linear slope within each cell, and uses this linear shape for calculations of the convection of fluid through the cell faces. The first step in this reconstruction scheme is calculating the position of the linear interface relative to the center of each partially-filled cell, based on information about the volume fraction and its derivatives in the cell. The second step is calculating the advected amount of fluid through each face using the computed linear interface representation and information about the normal and

tangential velocity distribution on the face. The third step is calculating the volume fraction in each cell using the balance of fluxes found during the previous step. In open channel flows, this interpolation scheme, permits to maintain a solid interface and only few cells have a value α different from 0 or 1.

2.4. Pressure based solver

2.4.1. Overview of pressure based solver

Fluent has two numerical ways to solve general equations, *pressure based* and *density based* solvers. The pressure-based approach is suitable for low-speed incompressible flows, while the density-based approach is mainly used for high-speed compressible flows. For VOF models, however, only the pressure based solver is available and the velocity field is obtained from the momentum equations. In this approach, the pressure field is extracted by solving a pressure, or pressure correction, equation which is obtained by manipulating continuity and momentum equations.

2.4.2. Discretization of continuity and momentum equations

Discretization of momentum equation Eq. (2-2) can be done using the same scheme of the general transport equation 2.2.3.. For example for the x-momentum the equation can be discretized from the pressure field and mass fluxes:

$$a_p u = \sum_{nb} a_{nb} u_{nb} + \sum p_f A \cdot \hat{i} + S \quad (2-11)$$

However these fields are not known a priori and must be obtained as a part of the solution through a series of correction on pressure and velocity fields.

Mass conservation equation Eq.(2-1) may be integrated over the control volume to yield the following discrete equation

$$\sum_f^{N_{faces}} J_f A_f = 0 \quad (2-12)$$

where $J_f = \rho \vec{v} \cdot \hat{n}$ is the mass flux through face f . The computation of the mass fluxes involve pressure and velocity field on the cell faces, therefore it is necessary to relate the face values of velocity, to the stored values of velocity at the cell centers. In order to relate face and center values one may use a pure linear interpolation scheme. The linear interpolation scheme results in unphysical checker-boarding of pressure. Hence, the velocity face values are not averaged linearly but weighted with momentum coefficients a_p from Eq.(2-11). Using this procedure, the face flux, J_f , may be written as

$$J_f = \rho_f \bar{v}_n \quad (2-13)$$

where the weighted average normal velocity is

$$\bar{v}_n = \frac{a_{p,c0} v_{n,c0} + a_{p,c1} v_{n,c1}}{a_{p,c0} + a_{p,c1}} \quad (2-14)$$

The subscripts $c0$ and $c1$ are referred to the cells on either side of the face.

2.4.3. Coupled solver

The pressure-based solver has a solution algorithm called *coupled solver* (in this case the PISO, Pressure-Implicit with Splitting Operators scheme), where the governing equations are solved in a coupled way. Since the governing equations are non-linear and coupled, the algorithm solves a system of equations which includes the momentum equation Eq.(2-11) and the pressure-based continuity equation Eq.(2-12). This solver is based on a degree of approximation between the correction for pressure and velocity higher than for other coupled solver. The remaining equations are solved in a decoupled fashion. The solution loop must be carried out iteratively in order to obtain a converged numerical solution. In the coupled solver each iteration consists of the steps outlined below

1. Update fluid properties (density, viscosity) including turbulent viscosity (diffusivity) based on the current solution.
2. Solve the momentum equations, and the pressure correction equation in a coupled way.
3. Correct face mass fluxes, pressure, and the velocity field using the pressure correction obtained from Step 2.
4. Solve the equations for additional scalars, if any, such as turbulent quantities, species, using the current values of the solution variables.
5. Check for the convergence of the equations.

2.4.4. Multigrid method

Fluent uses a multigrid scheme to accelerate the convergence of the solver by computing corrections on a series of coarse grid levels. The use of this multigrid scheme can greatly reduce the number of iterations and the CPU time required to obtain a converged solution particularly when the model contains a large number of control volumes. The direct matrix inversion is out of the question for realistic problems and solvers that rely on conjugate-gradient (CG) methods show robustness problems associated with the solution of the Navier-Stokes system. The numerical methods used are the iterative implicit solvers like Gauss-Seidel with preconditioner as ILU. Although the Gauss-Seidel and ILU schemes rapidly remove local (high-frequency) errors in the solution, global (low-frequency) errors are reduced at a rate inversely related to the grid size. Thus, for a large number of nodes, the solver “stalls” and the residual reduction rate becomes prohibitively low. Multigrid techniques allow global error to be addressed by using a sequence of successively coarser meshes. This method is based upon the principle that global (low-frequency) error existing on a fine mesh can be represented on a coarse mesh where it again becomes accessible as local (high-frequency) error. Since computations can be performed at an exponentially decaying expense in both CPU time and memory storage on coarser meshes, there is the potential for very efficient elimination of global error.

2.5. *Grid*

Grid domain is defined in Gambit, a specific program for mesh design. For open two-dimensional channel flows with regular geometry we can use a simple structured mesh with only two parameters measuring the grid in horizontal and in vertical direction. These parameters have to be determined according to the scale of the

interesting phenomenon. We need to define two different characteristic lengths for the two dimensions. For example, for two-dimensional wave like undular jump, the vertical characteristic length can be defined as the wave amplitude a_w and the horizontal one can be the wavelength L_w . We can define an adimensional quantity to correlate grid resolution Δx_i and length scale L

$$\delta_i = \frac{L_i}{\Delta x_i} \quad (2-15)$$

The index i is referred to the dimension which can be, in two-dimensional geometries, horizontal or vertical. The evaluation of the minimum value of δ is shown in the sensitivity analysis in 3.2.1..

A scale of the vertical wave amplitude can be estimated as follow

$$a_w \approx y_2 - y_1 \rightarrow \Delta y \approx \frac{a_w}{\delta_v} \quad (2-16)$$

However, aspect ratio of cells has to be limited, especially in our VOF model. Thus special constrain must be applied in order to have a good quality mass transfer at the interface. Therefore we need to have aspect ratio less than the free surface steepness shown in Eq.(2-17). In the undular jump, for example, we can estimate the wave steepness as follow

$$S \approx \frac{L_w}{2a_w} \quad (2-17)$$

$$\frac{\Delta x}{\Delta y} < S$$

This constrain is more restrictive, thus horizontal resolution has to be

$$\Delta x < S \frac{a_w}{\delta_v} \quad (2-18)$$

In the undular jump standard experiment S is approximative 5:1 but we will use a conservative value or 3:1 for the determination of the grid resolution. This yield that only δ_v have to be determined in the sensitivity analysis. Inside the commercial program Fluent, the refinement of the ROI (free surface and channel bottom) is possible in order to increase the precision of the interface and the near wall treatment.

2.6. Standard turbulence model

The standard model $k - \epsilon$ for momentum equation closure is applied. This model assumes isotropic turbulence. Transport equations for turbulence kinetic energy k and rate of dissipation of kinetic energy ϵ , which are valid mainly in the turbulent core flow, are solved. The turbulence equations can be written as

$$\frac{\partial}{\partial t}(\rho k) + \frac{\partial}{\partial t}(\rho k u_i) = \frac{\partial}{\partial x_j} \left[\left(\mu + \frac{\mu}{\sigma_k} \right) \frac{\partial k}{\partial x_j} \right] + G_k - \rho \epsilon \quad (2-19)$$

and

$$\frac{\partial}{\partial t}(\rho \epsilon) + \frac{\partial}{\partial x_i}(\rho \epsilon u_i) = \frac{\partial}{\partial x_j} \left[\left(\mu + \frac{\mu_t}{\sigma_\epsilon} \right) \frac{\partial \epsilon}{\partial x_j} \right] + C_{1\epsilon} \frac{\epsilon}{k} (G_k) - C_{2\epsilon} \rho \frac{\epsilon^2}{k} \quad (2-20)$$

In these equations, G_k represents the generation of turbulence kinetic energy due to the mean two dimensional velocity gradients

$$G = 2 \left(\left[\frac{\partial u}{\partial x} \right]^2 + \left[\frac{\partial v}{\partial y} \right]^2 \right) + \left(\frac{\partial u}{\partial y} + \frac{\partial v}{\partial x} \right)^2 \quad (2-21)$$

σ_k and σ_ϵ are the Prandtl number for k and ϵ and μ_t is the turbulent viscosity computed by combining k and ϵ as follows

$$\mu_t = \rho C_\mu \frac{k^2}{\epsilon} \quad (2-22)$$

Standard coefficient are used

$$\begin{aligned} C_\mu &= 0.09 \\ C_{1\epsilon} &= 1.44 \\ C_{2\epsilon} &= 1.92 \\ \sigma_k &= 1.0 \\ \sigma_\epsilon &= 1.3 \end{aligned} \quad (2-23)$$

Turbulence kinetic energy k and rate of dissipation of kinetic energy have to be defined manually on the boundary such as the velocity inlet and pressure outlet. An estimation of k and ϵ for boundary and initial conditions it is possible from the *turbulent intensity* I [18] which can be estimated from direct measurements in real channels

$$\begin{aligned} I &\equiv \frac{v'}{V} \\ k &= \frac{3}{2} (VI)^2 \\ \epsilon &= C_\mu^{3/4} k^{3/2} l^{-1} \end{aligned} \quad (2-24)$$

where V is the mean velocity, v' is root-mean-square of the unidimensional velocity fluctuations, l is the *turbulent length scale* that can be approximated with

$$l = 0.07 y_c \quad (2-25)$$

2.7. Wall functions

To simulate no-slip conditions and turbulent effects, Fluent provides wall functions that complete the standard turbulence model in regions close to walls. For undular jumps, walls are the major turbulent source and therefore, is really important an accurate simulation in this region. Numerous experiments have shown that the near-wall region can be largely subdivided into three layers. In the innermost layer, called the “viscous sublayer”, the flow is almost laminar, and the (molecular) viscosity plays a dominant role in momentum transfer. In the outer layer, called the fully-turbulent layer, turbulence plays a major role. Finally, there is an interim region between the viscous sublayer and the fully turbulent layer where the effects of molecular viscosity

and turbulence are both important [18]. Fluent wall functions simulate these three layers according with the grid resolution and k , ϵ , mean velocity are all taken care of by these functions. Roughness effects are not simulated by standard wall functions thus, the walls are smooth.

3. Undular jump simulation

3.1. Numerical modelling

3.1.1. Introduction to undular jump simulation

Undular jump simulation aims to reproduce the well known phenomenon with Fluent (see 1.3.2. for definition). In an horizontal channel, a supercritical flow becomes subcritical making stationary waves, an undular jump (sketch in Fig 3-1). With these simulations we want to validate the model and perform systematic sensitivity analysis. Upstream and downstream free surface depths must follow Eq.(1-15) for momentum function balance. In order to compare the simulations with experimental data, we set the upstream Froude number equal to 1.6. We assume that the undular jump is a two dimensional phenomenon thus we work with a two dimensional grid placed in a vertical longitudinal section ideally in the middle of a wide channel. Numerical grid cover the main part of the undular phenomenon, approximatively three wavelength, and a little part of the supercritical inflow. In a real channel, the flow transformation from supercritical to subcritical can happen in different ways farther downstream. Fluent can simulate a downstream boundary with a pressure condition that simulate a flow with a subcritical depth (see 3.1.5.). In paragraph 3.2.2. we perform an analysis on the placement of the grid domain to exclude any dependence of the solution. Even if really realistic and detailed conditions can be used, we always prefer *simplicity* if the results are comparable. Thus, conditions ensemble has to reproduce real experiment and has to be as simple as possible at the same time. Detailed analysis of necessary complexity introductions are showed below.

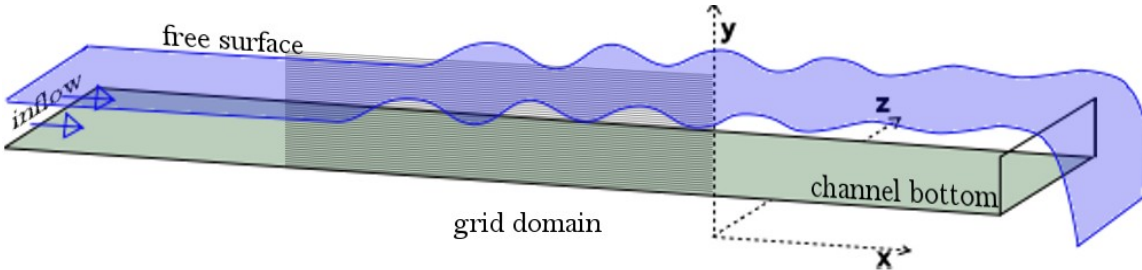


Fig 3-1: Open channel sketch with undular jump. Dark surface indicate grid domain. Dotted line indicate reference system.

3.1.2. Operating conditions

In Fluent, operating conditions are gravity and atmosphere effects. Gravity is on, $g=9.81 \text{ m/s}^2$ downward direct and the pressure is the standard at the the sea level $p_0=101325 \text{ Pa}$. We must also define an operating density for the gas phase because temperature is not a variable of the model. It's therefore fixed at the average value of air at sea level $\rho_0=1.225 \text{ kg/m}^3$. Fluent use a redefined pressure as

$$p' = p - p_0 - \rho_0 g y \quad (3-1)$$

Thus, quiet air in the channel has a $p'=0$ and quiet water has a vertical hydrostatic pressure profile.

3.1.3. Boundary: velocity inlet

Inlet boundary conditions are fundamental for the definition of the problem. Fig 3-2 shows velocity inlet placement in the grid domain. The velocity inlet has a fixed height that is about a third of the channel height and only water come out with normal velocity. The simplest choice is a vertical constant velocity profile. Constant velocity however does not yield a simulation of the undular jump (see 3.4.1.). Thus, in order to simulate a more reliable fully develop profile, we use Eq.(3-2).

$$V(y) = V_{max} \left(\frac{y}{y_{max}} \right)^{\frac{1}{N}} \quad (3-2)$$

Fluent requires a special user define function “*udf*” wrote in c++ language to define an arbitrary profile (see Appendix B). Experiments show that N can vary from 6.9 to 8.8 for smooth wall regular channels [23]. Using this profile, momentum coefficient β , can be calculated from Eq.(1-5) and become

$$\beta = \frac{\left(\frac{1}{N} + 1 \right)^2}{\left(\frac{2}{N} + 1 \right)} \quad (3-3)$$

For value of N in the range from 5 to ∞ , the coefficient will be approximated to unit. Out of this range, the approximation can't be done and we need to consider this coefficient in the momentum function balance equation. In paragraph 3.4.1. we perform sensitivity analysis to study the affection of N variations.

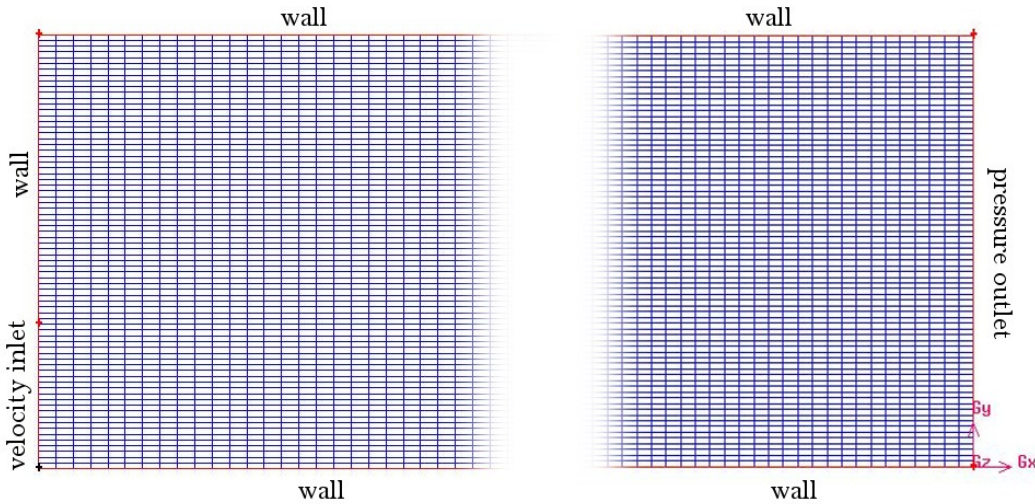


Fig 3-2: Boundary and grid sketch of the initial and final part of the grid domain. Flow direction from left to right.

3.1.4. Boundary: turbulent inlet quantities

Turbulent kinetic energy and turbulent dissipation rate have to be defined at the inlet. As a first approximation we define a null turbulent intensity and leave the model creates turbulence from shear and vorticity of the flow. We use this option if nothing

else is indicated according with the simplicity criteria. This option will be compared with a fully turbulent flow according with experimental data in paragraph 3.2.3.. The affection of the turbulence is not negligible if large amount of energy are involved as we will see in paragraph 3.4.2..

3.1.5. Boundary: pressure outlet

Pressure outlet is the other key boundary for undular jump simulation. Fluent provides a special pressure outlet specific for open channel flow that requires the free surface height from the channel bottom. This boundary is placed along all the right wall (Fig 3-2) and is in contact with both phases. Static pressure at the boundary, for subcritical flow, is determined as follow

$$p'(y) = (\rho - \rho_0) |\vec{g}| (y - y_{fs}) \quad (3-4)$$

where y_{fs} is the *free surface position* and p' is the redefined pressure (see 3.1.2.). We will set in all simulations the free surface position at y_2 in order to simulate subcritical flow according with momentum function balance Eq.(1-15). If static pressure next to the boundary is less than the fixed one, reverse flow of gas phase with normal direction can occurs. In steady condition reverse flow under the flow depth doesn't occur because the pressure at the boundary results equal to the required one. This boundary doesn't fix the free surface but only creates a pressure that make this happen, so it's not a direct constrain for free surface undulations. Ideally this boundary have to be placed far from the jump, where undulations are attenuated. For calculation cost reason it will be placed closer, approximatively 3 wavelength from the jump. The analysis of this problem shows that effects are negligible in paragraph 3.2.2..

3.1.6. Standard channel

Now, we can define few parameters to create a standard channel to use for all simulations that yields the undular jump phenomenon. This standard channel will be the simplest as possible to reproduce an undular jump with Froude number comparable to the experimental data of Chanson (2005) [24]. We will perform variations to some of these parameters to study sensitivity. Without specific indications, numerical simulations use standard channel.

Flow:

- Froude number: 1.6
- critical depth: 0.276 m
- critical velocity: 1.65 m/s
- discharge: 0.456 m²/s

Grid domain:

- dimensions: 6 m long and 0.6 m high
- resolution: defined in each simulation

Boundary:

- velocity inlet: 0.2 m high from the bottom, mean velocity = 2.28 m/s, velocity profile following Eq.(3-2); null turbulence kinetic energy and dissipation rate
- pressure outlet: 0.6 m high; free surface level = 0.37 m ; return flow with null turbulence kinetic energy and dissipation rate

We expect scale invariance, thus all length will be compared with the characteristic

quantities of the flow (critical depth or critical velocity).

3.2. Model validation

In this section we want to perform some test to validate the model and ensure that the result doesn't depend upon arbitrary choice made in the definition of the numerical model parameters. We want also to compare the simulations results with a similar experiment in real channel.

3.2.1. Grid sensitivity

Grid resolution is probably one of the most critical numerical parameter in the VOF simulations. The model doesn't resolve turbulence fluctuations and thus they don't represent a big issue in determining the grid resolution. Wall functions require conditions for the wall adjacent cells to perform reliable results that are in general respected in the simulations performed in this work. Thus, the only issue seems to be represented by the phenomenon scale that must be well resolved by the grid. We already discussed how the length scale can be found for the undular jump and which other constrains we need to take in account (see paragraph 2.5.). However the minimum number of points for length scale must be determinate with systematic tests on the model. Therefore in this paragraph we perform a systematic sensitivity analysis to determinate only the vertical grid resolution δ_v since the horizontal is given by Eq.(2-17). We now define a set of resolutions and we test them with the same models and boundary conditions and keeping the aspect ratio always 3:1. Fig 3-4 shows the free surface data simulations for the different resolutions. To compare the data, we have performed a x-offset in order to superimpose the first crest. As introduces so far, after a fast visual analysis we can conclude that grid resolution is a fundamental parameters for VOF simulations. Under a certain threshold, we can estimate around $\delta_v < 20$, the results are poor and not reliable because wave attenuation is overestimated and free surface undulations are not resolved with enough points. Over this threshold the results are more reliable and the undular jump characteristic can be recognized. Free surface appears closer to experimental data and a resolution increment doesn't yield big changes in the results.

In order to give a quantitative analysis of this behavior, we can define a distance between the free surface profile and the ideal one. We take the higher resolution profile $\delta_v = 85$ as reference and the distance can be defined as follow:

$$d_{85} = \frac{\left(\sum_{i=1}^N (y_i - y_{85})^2 \right)^{\frac{1}{2}}}{N a_w} \quad (3-5)$$

where y_i represent the i^{th} value of the free surface profile and the subscript 85 identify the linear interpolation of the higher resolution free surface profile over the x coordinate of the coarse resolution. N is total number of points in the coarser resolution and a_w is the wave amplitude.

Fig 3-3 shows the normalized distances defined by Eq.(3-5) over the grid resolution. As we can see, after a threshold, the distance is stable on a fixed value. Over this threshold the model doesn't converge uniformly into a single solution. The solution is not an attractor and small differences in the algorithm yield small differences in the

solution. This means that improving the resolution over this threshold, with increase of calculation cost, could not yields significant quality improvement of the solution. Thus, we can say for the undular jump simulation δ_v has to be bigger than 20.

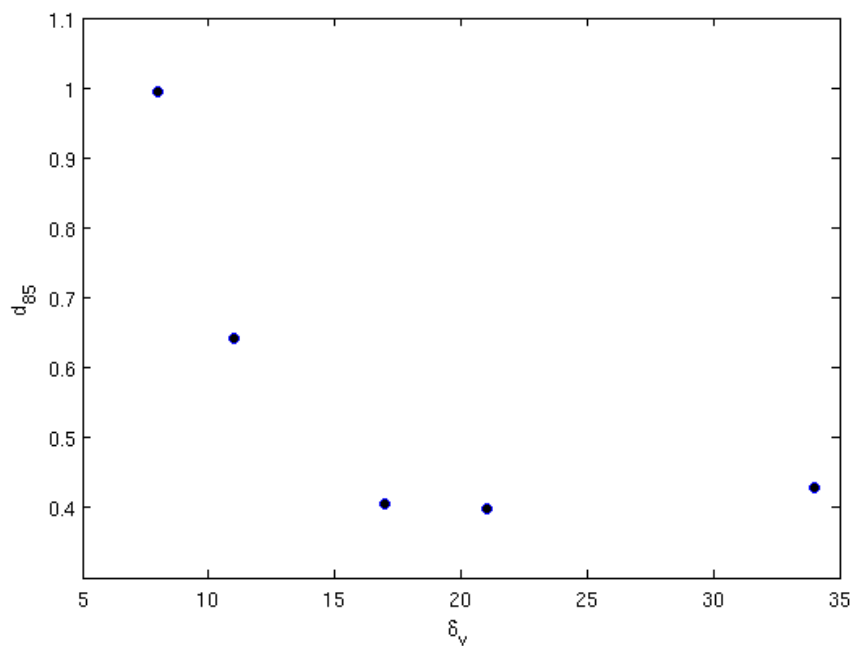


Fig 3-3: Distance between free surface profile of $\delta_v=85$ and different resolutions

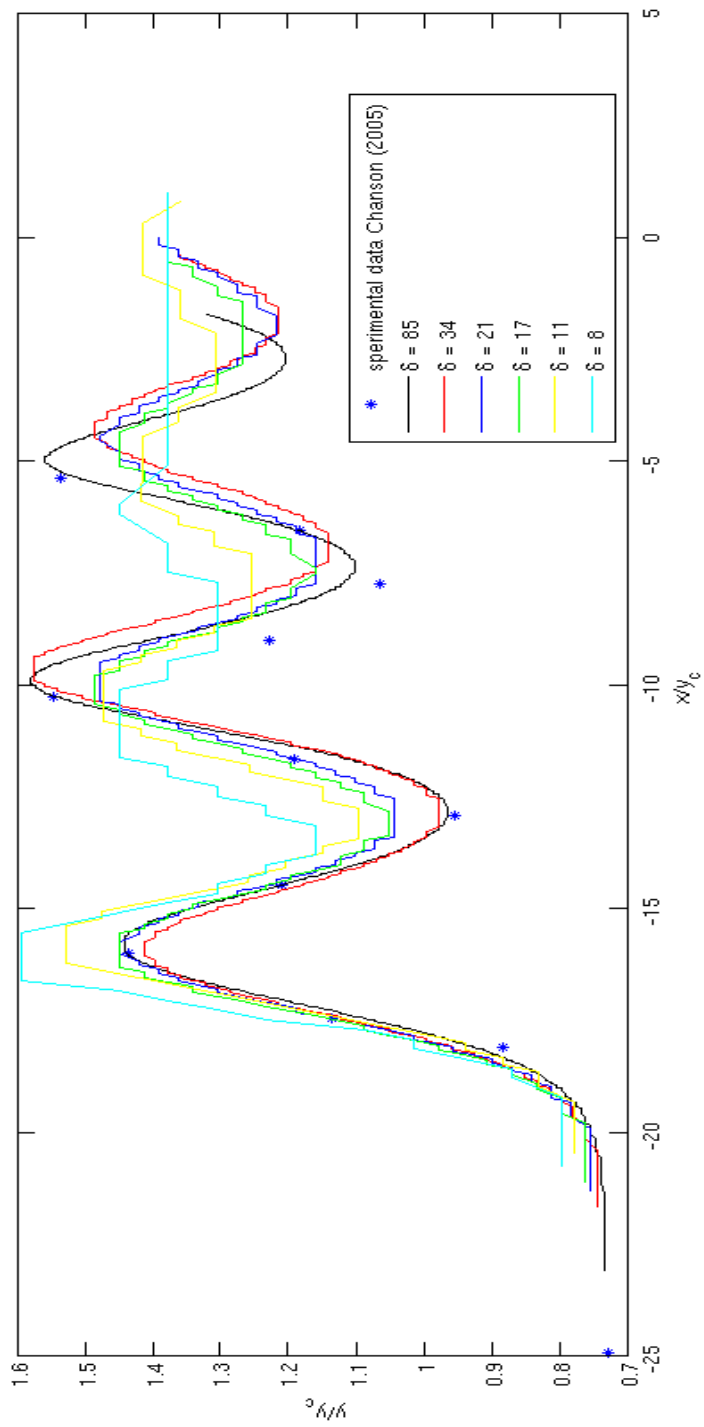


Fig 3-4: Free surface data comparison. Different colors indicate different resolutions

3.2.2. Outlet sensitivity

Pressure outlet boundary ideally has to be placed far from the wavy section of the simulation to avoid numeric artifact. In subcritical flows, downstream boundary is responsible of the undular jump formation and its role is fundamental. For computation cost reasons, we cut the grid domain after 3 wavelength. Thus, we need to demonstrate that this choice doesn't affect significantly the simulation result. Fig 3-5 shows free surface profiles for identical simulations except for the domain length. The extended domain ends where wave amplitude reaches the grid resolution and the standard domain ends after 3 wavelength according with the standard model. The results are similar but at the end of the standard domain little differences are visible and the wave amplitude is weakly attenuated. The outflow boundary can therefore interferes with the solution but the differences are comparable with grid resolution except that in a region next to the boundary in which we can't consider the results reliably. Therefore a short domain is preferred for the smaller computation cost.

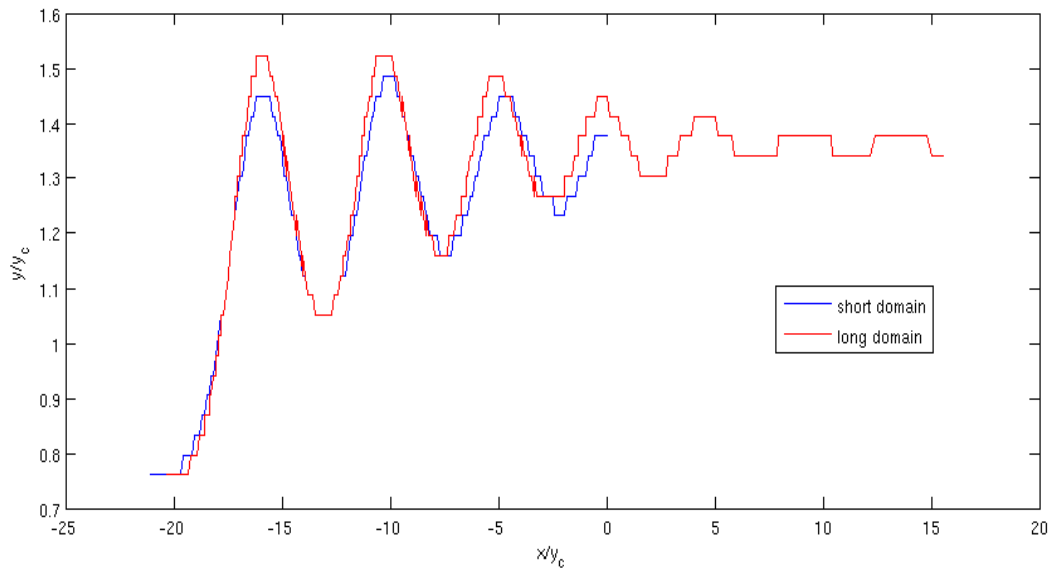


Fig 3-5: Free surface comparison between a short and a long domain. $Fr=1.6$; $Res \delta_v=21$;

3.2.3. Turbulent inlet sensitivity

We want now to make sure that the null turbulence simplification doesn't affect much the simulations result. Thus we compare a null turbulence simulation with a more realistic turbulent profile derived from experimental data. Chanson and Brattberg (1997,2000 [20],[21]) performed experiments for fully turbulent condition in a horizontal channel without hydraulic jump. We assume that turbulent intensity is not affected strongly by the Froude number. Tab 1 shows turbulent intensity I measurements.

$y_{\max} =$	0,014 m	y/y_{\max}	I
$q =$	0,033 m ² /s		v'_x/V
$b =$	0,25 m		(%)
$Fr =$	6,3	0,12	7,76
		0,19	7,34
		0,26	6,36
		0,33	4,61
		0,40	4,5
		0,48	4,93
		0,55	2,71
		0,62	3,91
		0,69	2,23
		0,76	2,74
		0,83	2,44

*Tab 1: Experiment by Chanson and Bratteberg (1997,2000).
Are indicated turbulent intensity measurement and channel
conditions*

From Tab 1 data we calculate a linear interpolation for I profile (Fig 3-8) and we define a function Eq.(3-6) that gives the turbulent intensity for a fully develop flow as follow

$$f_I\left(\frac{y}{y_{\max}}\right) = p_0 + p_1\left(\frac{y}{y_{\max}}\right) \quad (3-6)$$

$$p_0 = 8.1 \quad p_1 = 7.7$$

Using Eq.(3-6), Eq.(2-24) yields the profiles for turbulent quantities

$$f_k(y) = \frac{3}{2}(V f_I(y))^2 \quad (3-7)$$

$$f_\epsilon(y) = C_\mu^{3/4} V^{-1} (f_k(y))^{3/2}$$

These functions are implemented for Fluent use in Appendix B in the *udf* file.

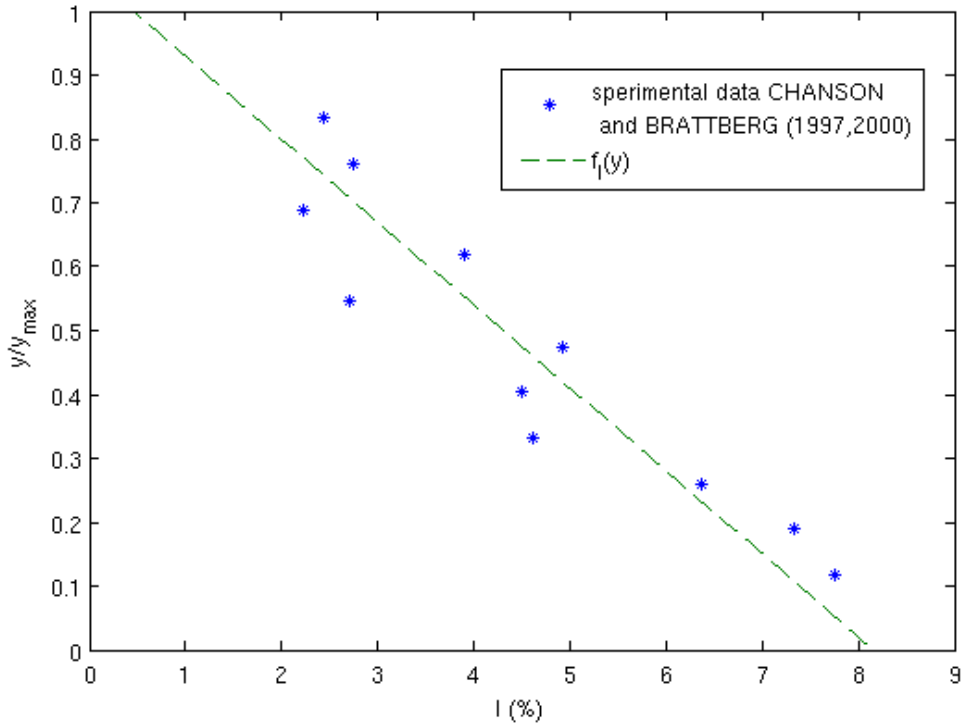


Fig 3-6: Linear interpolation of experimental data to define a vertical turbulent intensity profile

Fig 3-7 shows a comparison between a null-intensity turbulent profile and the experimental profile defined by Eq.(3-6). The differences of the free surface profiles are not significant and can be, at this level, neglected. Turbulent kinetic fields show also that k for the experimental profile has the same order of magnitude of the one produced in the turbulent core when no turbulence is provided at the inlet. Values of

$k-\epsilon$ in the flow core are substantially the same. Analysis of velocity and pressure profiles give similar negligible differences. Thus, differences are small between these two simulations and according with the simplicity criteria the null turbulence profile is preferable for simulations as turbulence at the inlet is not a necessary condition for the undular jump formation.

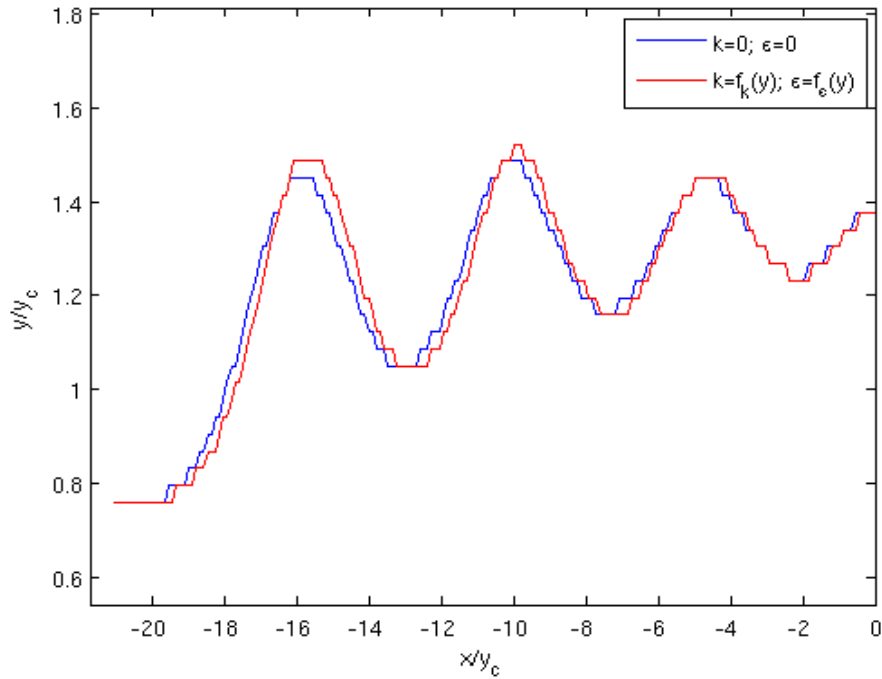


Fig 3-7: Free surface profile for different turbulent inlet. Res $\delta_v=17$;

3.2.4. Undular jump experiment

A comparison with a real experiment is now essential. Undular jump experiments have been performed from different authors. Unlucky we haven't found the perfect experiment without three dimensional effect involved. Thus, we take the closest to our numerical simulations. It's important to note that the numerical simulations have been performed before and independently from the knowledge of the experimental results. In numerical model, Froude number only have been tuned to permit the comparison with the experiment data. The closest experiment has been done by Chanson (2005) [24] for studies about undular tidal bore sediment transport in estuarine. For this study the author use a stationary undular jump experiment to study bottom stress. We are interest in free surface and various profile data of the experiment called "HQ2". Experiment main parameters are shown below:

Undular jump:

- Froude number: 1.57
- channel width: 0.5 m
- critical depth: 0.11 m
- critical velocity: 1.02 m/s
- discharge: 0.055 m³/s (0.11 m²/s)

Boundary:

- velocity inlet: 0.08 m high from the bottom, low turbulence kinetic energy, mean velocity = 1.37 m/s

The channel has an aspect ratio of about 5. Thus three dimensional effects cannot be forgotten. The central section of the channel is taken as the most representative of a two dimensional flow for comparison. Inflow condition was controlled by a vertical sluice gate and downstream conditions with a far dam (Fig 3-8).

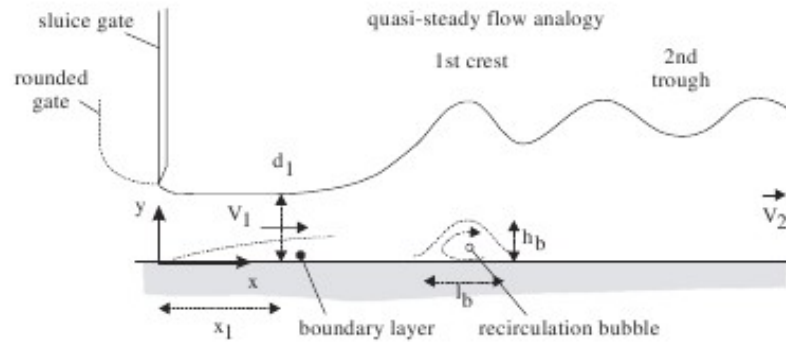


Fig 3-8: Experiment sketch

Standard channel for numerical simulation (3.1.6.) represent these conditions with for a scale factor of about 2.5. Comparison with such scale factor demonstrate a scale invariance at the same time.

3.2.5. Free surface data comparison

Fig 3-9 shows free surface data for numerical model and real experiment (see 3.2.4.). An x-offset has been performed to overlap horizontally first wave crest. The free surface shapes are really close and wavelength and wave amplitude are simulated correctly especially in the first two waves. At the end of the grid domain there are bigger differences in longitudinal placement of the free surface. This effect might be caused by the numerical boundary (see 3.2.2.) but also from side boundary layers that necessarily occur in a real lateral bounded channel and interfere with the central flow. This comparison shows a good agreement and also that a two dimensional analysis can be useful in order to simulate regular channels.

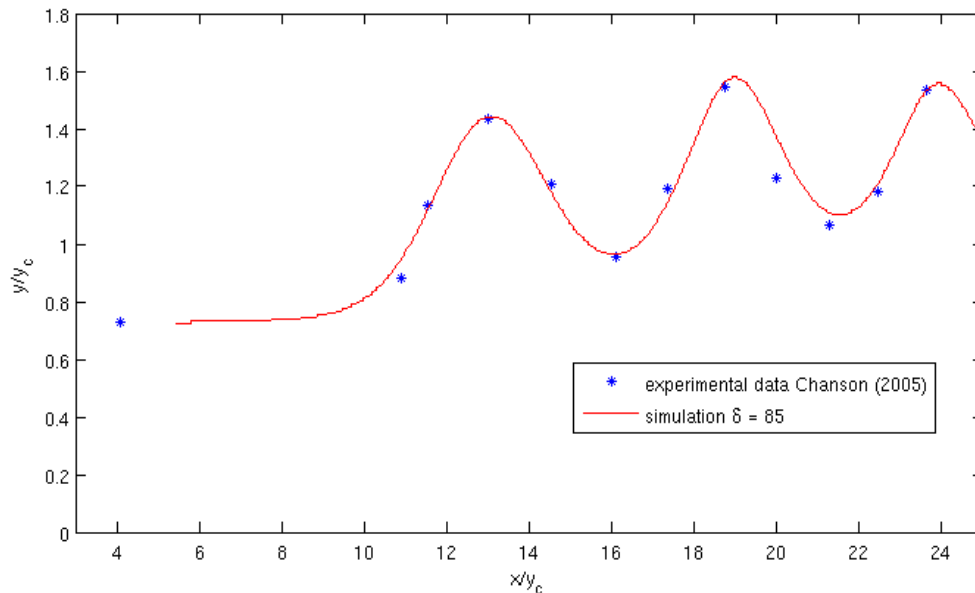


Fig 3-9: Free surface profile comparison between standard Fluent simulation and experimental data. Res $\delta_v=85$

3.3. Undular jump fields

3.3.1. Velocity fields

Numerical model provides velocity fields for the whole channel. A strong gradient characterizes the interface between the phases, making easy the identification of the free surface. Velocity field for x-velocity (Fig 3-10) permits to identify clearly the *recirculation bubble* underneath the first crest. This zone has a low, or slightly negative, horizontal velocity acting like a solid boundary. The gradient between the main flow and this zone is strong and is a powerful source of vorticity and turbulence. Recirculation zones are also visible under the successive crests, even if their behavior become weaker moving downstream. The organization of the flow in a solid stream is evident and maintained through the waves. Turbulent dissipation effect tends to break this organization moving downstream. Velocity field for y-velocity (Fig 3-11) gives a clear idea of the undular features and of the attenuation.

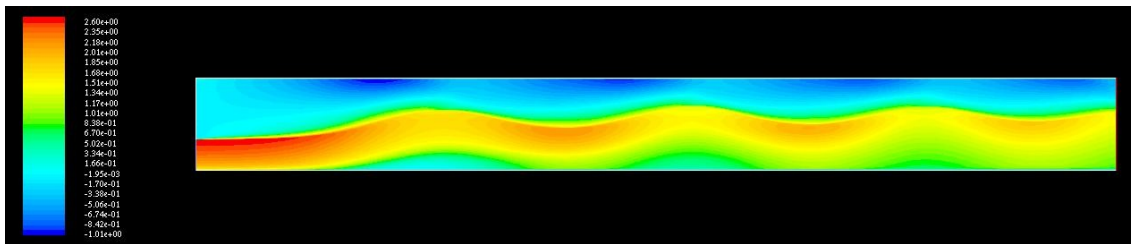


Fig 3-10: x-velocity (m/s) field. Res. $\delta=85$

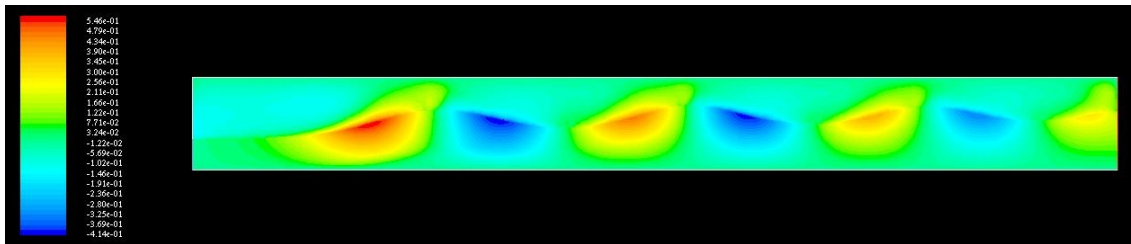


Fig 3-11: y-velocity (m/s) field. Res. $\delta=85$

3.3.2. Static pressure profiles

Free surface curvature has a strong affection on static pressure vertical profiles. In open channels, where the surface is straight, the pressure profile is superimposed to the hydrostatic one (Fig 3-12). Vertical pressure profile, in convex curvature with the center in the water, is lower than the hydrostatic (Fig 3-13 and Fig 3-15). In reverse, concave curvature has a larger pressure than hydrostatic (Fig 3-14). This is due to the total energy conservation law (see [35] for details). Experiment data for all the vertical profiles showed in Fig 3-12, Fig 3-13, Fig 3-14, Fig 3-15 seem to follow more or less closely the simulations. Upstream hydrostatic profile is simulated better than any other because depend only upon the upstream conditions. Successive profiles, like the free surface data, have small differences due probably to three dimensional effects or differences in inflow conditions.

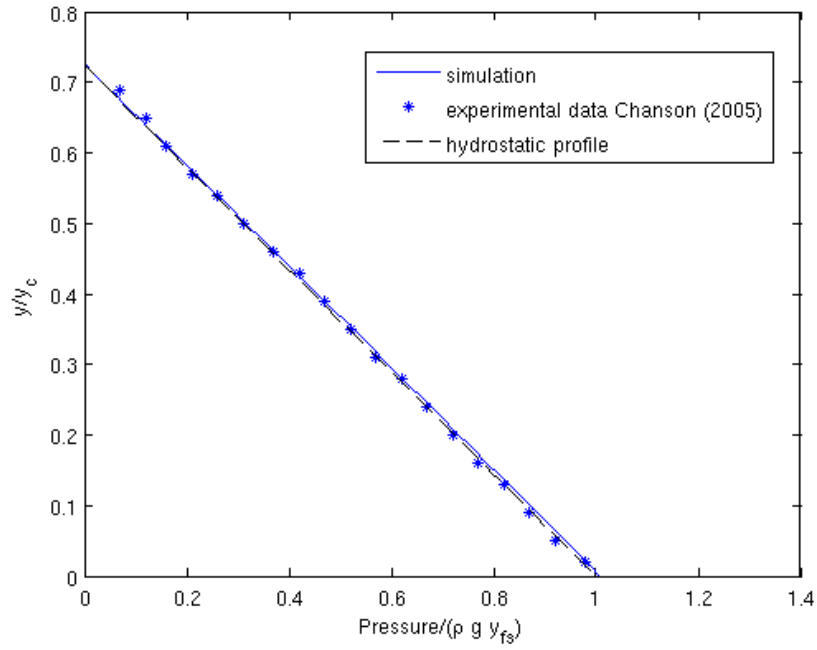


Fig 3-12: Pressure profiles for upstream flow (velocity inlet). Res $\delta_v = 34$

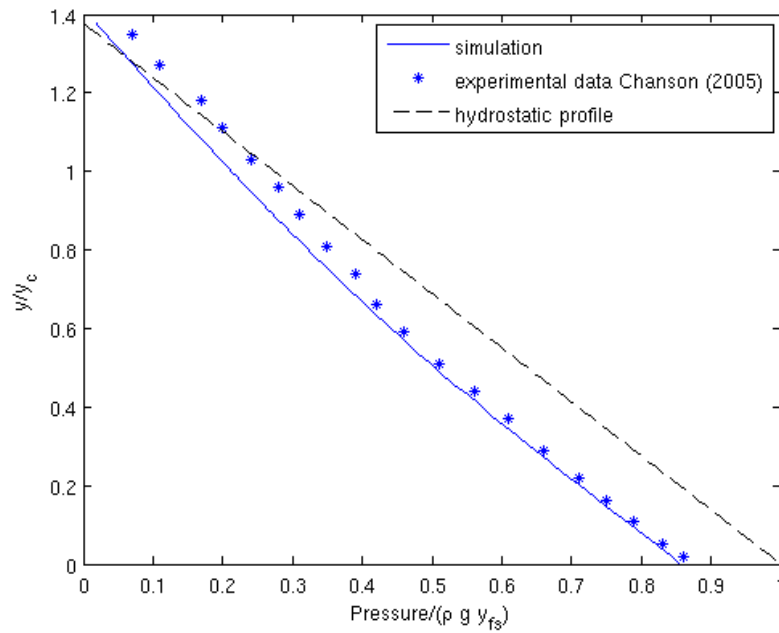


Fig 3-13: Pressure profiles, top of the first crest Res $\delta_v = 34$

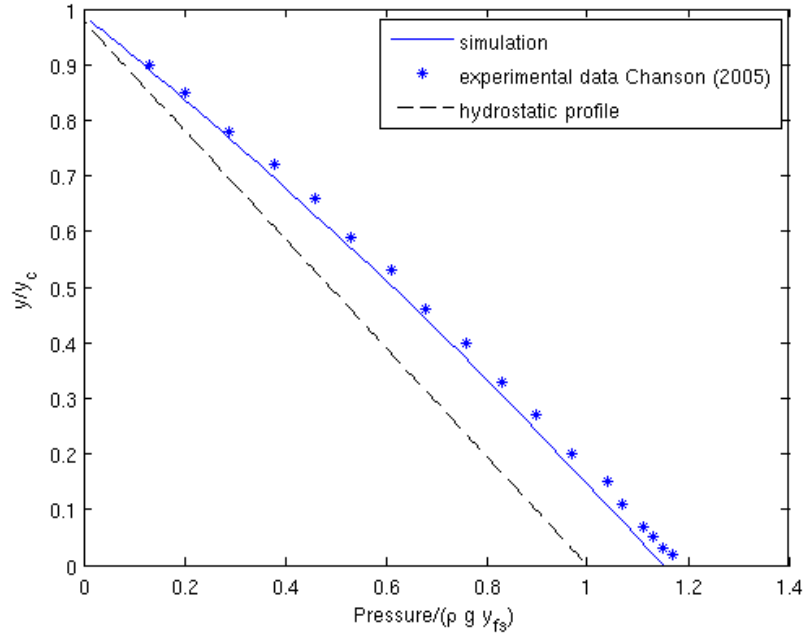


Fig 3-14: Pressure profile, bottom of the first trough Res $\delta_v=34$

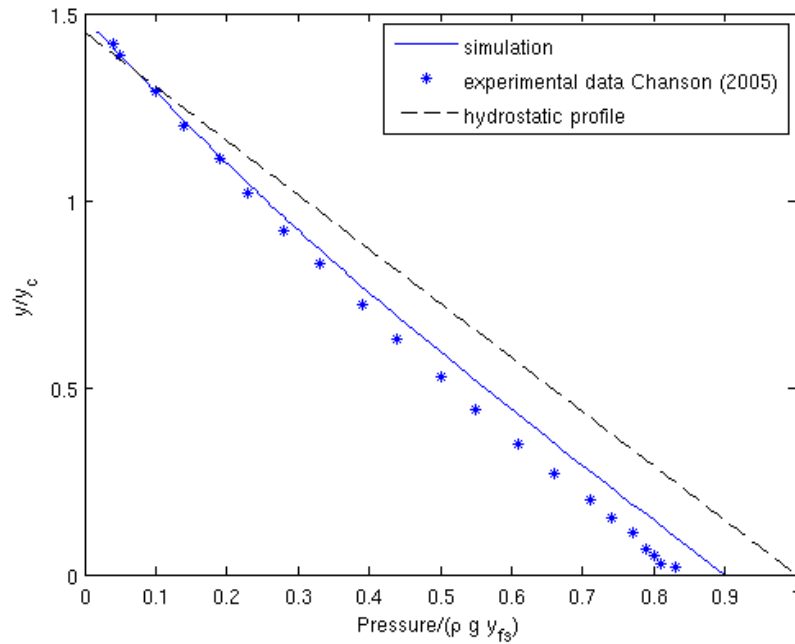


Fig 3-15: Pressure profile, top of the second crest, Res $\delta_v=34$

3.3.3. Vorticity field

Numerical simulation for standard channel yields vorticity field in Fig 3-16. At steady state, the vorticity is created underneath the first wave crest in the recirculation bubble. In this zone, the fully develop boundary layer is detached from the channel bottom and the consequent shear is identified by the large presence of vorticity. Downstream the first crest, the vorticity tends to decrease along the channel to recreate a developed turbulent flow. The friction between the two phases at the interface is also a small and negligible source of vorticity but still visible in Fig 3-16.

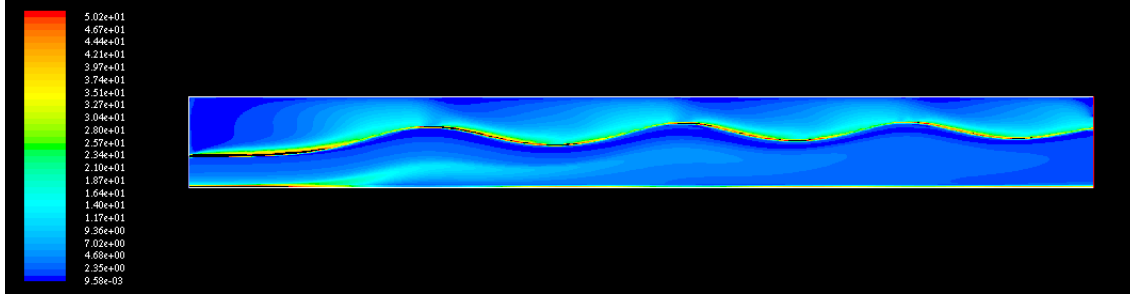


Fig 3-16: Vorticity field (1/s). Res: $\delta_v = 34$

3.4. Undular jump sensitivity analysis

In next paragraphs we want to study how the undular jump is sensitive to the inlet conditions. We also try to fix a thresholds over which the wave breaks and the flow turns upstream with foam formation and air entrainment. We refer to this threshold as *critical* because over it, the flow forms a completely different pattern, the direct jump.

3.4.1. Velocity inlet profile

Upstream conditions, above the numerical domain, determine the curvature of the velocity profile at the inlet boundary. Therefore, in the numerical model, we need to define arbitrarily the inlet conditions. In regular and straight channels, friction with the bottom creates a steady vertical shear that can be approximated with Eq.(3-2) reported below:

$$V(y) = V_{max} \left(\frac{y}{y_{max}} \right)^{\frac{1}{N}} \quad (3-2)$$

The profile at the inlet may changes with respect to bed roughness or any other source of turbulence. In this paragraph, we want to understand how the curvature of the profile modify the undular free surface. Therefore we run different simulations modifying the coefficient N and keeping constant the resolution and the standard conditions. Under a certain N value, the approximation of β coefficient to unit it's not acceptable anymore and we need to recalculate the pressure outlet level to keep the momentum function balance. For example, in a simulation for $N=3$ the pressure outlet has been recalculate and thus the results are not directly comparable. Increasing

N , the wave steepness increase until and over a critical threshold, the wave reach the critical state and become a direct jump. We have simulated an undular jump with $N=11$ keeping the solid interface and with an high degree of instability (see 3.4.4.), but over this value only direct jump have been found at steady state. Thus, to better understand the sensitivity to the velocity profile, we want to study the range

$5 \leq N \leq 10$ in which the standard conditions can be used and the steady state has a solid surface. Fig 3-17 shows the profiles for different N values that has been used in the simulations to give an idea of the profile shapes. Fig 3-18 shows the free surface profiles for the simulations in the non-critical range. As we can see, the wave amplitude increase incrementing N while wavelength decrease. Thus, wave steepness increase if the profile has less curvature. This feature is consistent with the existence of an upper threshold of N over which the wave breaks because the steepness overtake the critical value. This analysis is however related to the standard conditions and we can't generalize the thresholds.

An experiment performed on small Froude number ($Fr=1.2$, $N=20$), has shown that for large N value the wave tends to break anyway even if the expected wave amplitude is small. This behavior may suggest that the smooth undular jump is maintained through the flow organization. If the velocity inlet profile is already organized with a good vertical shear, the formation of the smooth surface is easier. Instead, if the profile is not vertical organized, the flow tends to go underneath the slower subcritical flow yielding the formation of a direct jump. Thus, the threshold may varies with the Froude number but a detailed evaluation needs to be done in future studies.

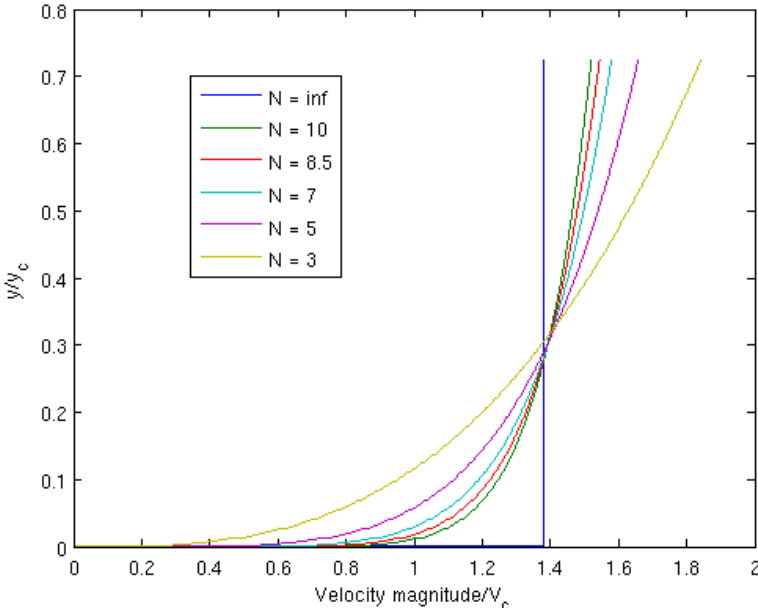


Fig 3-17: Velocity inlet profiles for different N following Eq.(3-2)

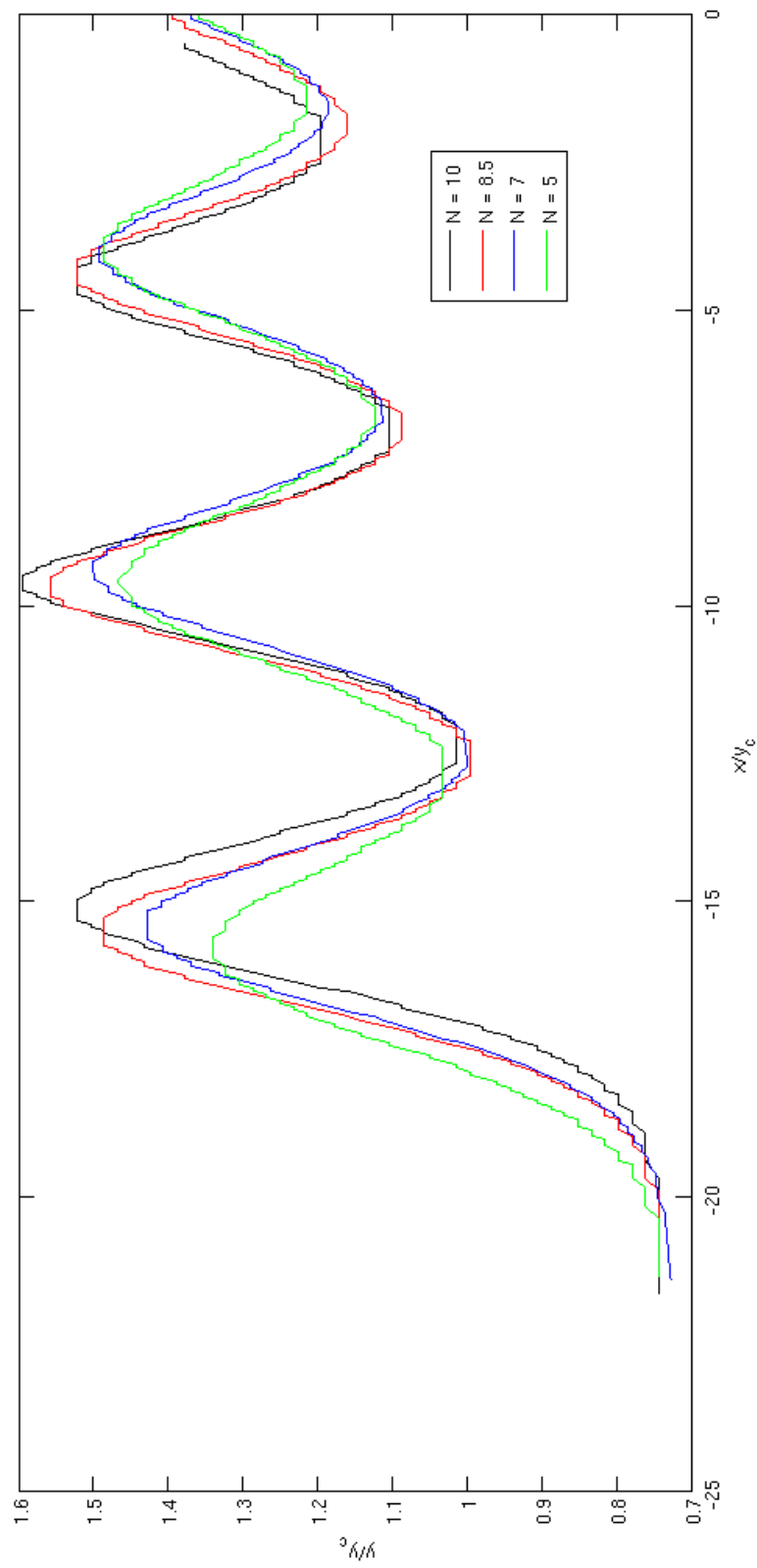


Fig 3-18: Free surface profiles for different N value. Res $\delta_v = 34$

3.4.2. Turbulent kinetic energy

At the inflow, turbulent kinetic energy has to be determined from upstream streaming conditions. For example, a smooth regular straight channel must have a lower turbulent intensity than a rocky river bed with same mean velocity. The problem is how the turbulent upstream conditions, without modifying the inlet velocity profile, can affect undular jump. Experiments in order to study this issue, are difficult to set up. Some experiment performed with rough walls were performed by CHANSON (1994) [23]. He concluded that wall roughness, and thus turbulence, affects undular jump velocity field and the free surface in a not trivial way. Numerically working, this analysis is quite easy to perform, we can test five different turbulence inlet to study sensitivity. Considering Eq.(3-7) that relate the turbulent intensity to the other turbulent quantities, five vertical profiles for k and ϵ are obtained from a set of multiplier coefficient (see Eq.(3-8)) using the experimental turbulent intensity profiles function f_I defined in Eq. (3-6).

$$c_I f_I(y) \text{ with } c_I=0,1,2,3,4 \quad (3-8)$$

Leaving all other parameters constant at the standard conditions, the model simulate undular jump for $c_I=0,1,2,3$. For these values, the higher is the turbulence at the inlet, the higher is the wave amplitude (see Fig 3-19). With higher turbulence, $c_I=4$ the critical state is reached yielding a direct jump.

Differences in inlet turbulence substantially change k field along the channel (Fig 3-20). As showed in Fig 3-20, in the first part of the channel a large fraction of the incoming turbulence is dissipated because no turbulent sources are present. However, a consistent part of turbulence reaches the main part yielding different flow organizations and modifying the free surface profile. At reverse, when no turbulence is supplied at the inlet, turbulence sources exist just under the first crest when the main flow is detached from the channel bottom and velocity shear is strong. Thus, high turbulence yields more instability for the smooth waves. Kinetic energy is therefore a parameter with a critical threshold over which the wave instability can be found. However, it's possible to reach this critical threshold only with high turbulence level, around four time the turbulence of a smooth channel.

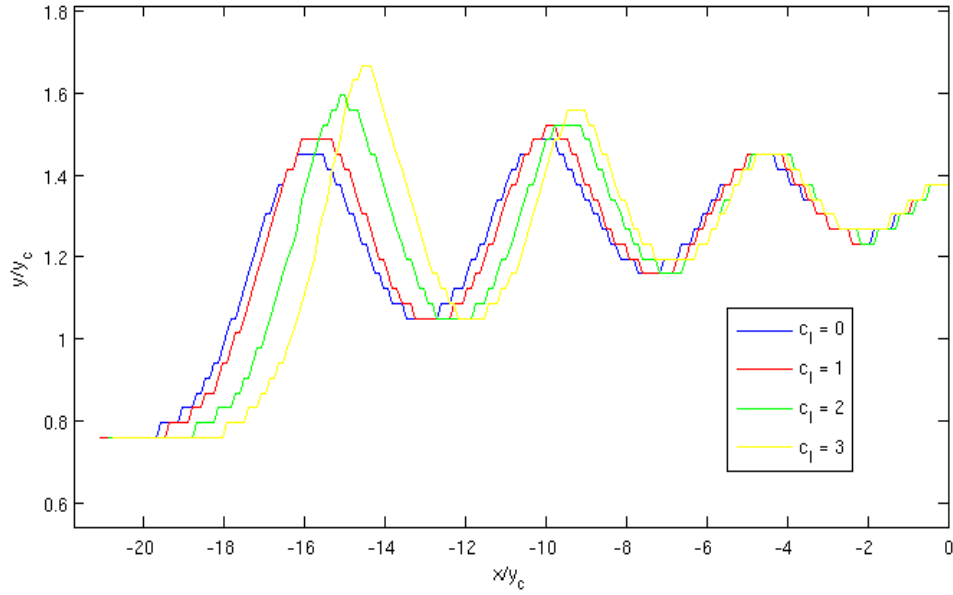


Fig 3-19: Free surface profile comparison with different turbulent inlet profiles

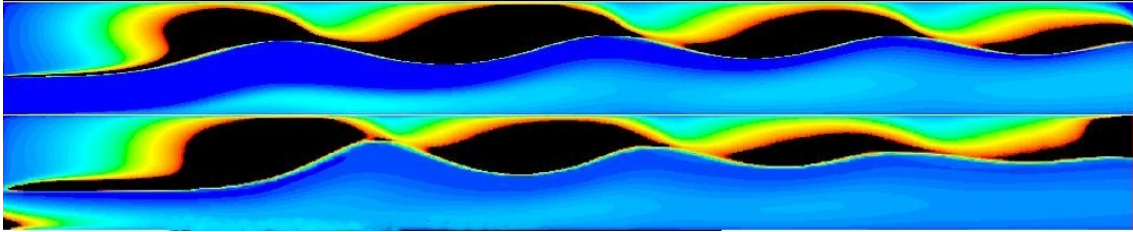


Fig 3-20: k fields along the channel respectively for $c_1=0$ and $c_1=3$. Color scale is the same for both fields and goes from $k=0$ to $k=0.02$, black color means out of scale.

3.4.3. Froude number

The upstream Froude number is the characteristic parameter to define the intensity of the phenomenon. For $Fr=1$ the flow is critical and no undulations occurs. If

$Fr > 1$ the inflow turns from supercritical to subcritical, therefore a positive surge occurs. The amplitude of the waves is expected to increase with Fr because depends somehow from the difference between y_1 and y_2 . We expect also an upper threshold where the wave breaking occurs and the undular jump turns suddenly in a direct jump. After several simulations we have identified the characteristic Froude number undulations disappearance at $Fr=1.9$ for the standard channel. Others authors agree that this threshold is placed in a range from 1.5 to 4 [24] with dependency on the aspect ratio of the channel. After the studies on the velocity inlet profile and on turbulent kinetic energy (see paragraphs 3.4.1. and 3.4.2.), the large degree of uncertainty on the determination of the threshold could be explained by the fact that the undular jump is strongly influenced by the inflow conditions, and in real channel, from lateral effects too. Therefore, we need to associate to this threshold for a wide channel, the velocity and the turbulent kinetic energy profiles; in this case velocity profile is defined in Eq.(3-2) with $N=7$ and no turbulent kinetic energy at the inlet (standard channel).

Fig 3-23 shows all the free surface profiles for the simulations performed in the range from $1.3 < Fr < 1.9$. We observe that wave amplitude increase with increasing Froude

number while wavelength decrease. Fig 3-21 pinpoints that dimensionless wave length slightly decreases with differences encompassed in a 10%. Fig 3-22 shows how wave amplitude increases almost linearly with Froude number. The comparison of these results with the Boussinesq analytic solution haven't yielded any satisfactory approximation of the behavior of wave characteristics. This two quantities have been studied from different authors in real experiments (see review at [22]) but the results are spread and don't identify a clear behavior. We think that the experimental data spread can be explained again with the dependency from the inflow conditions.

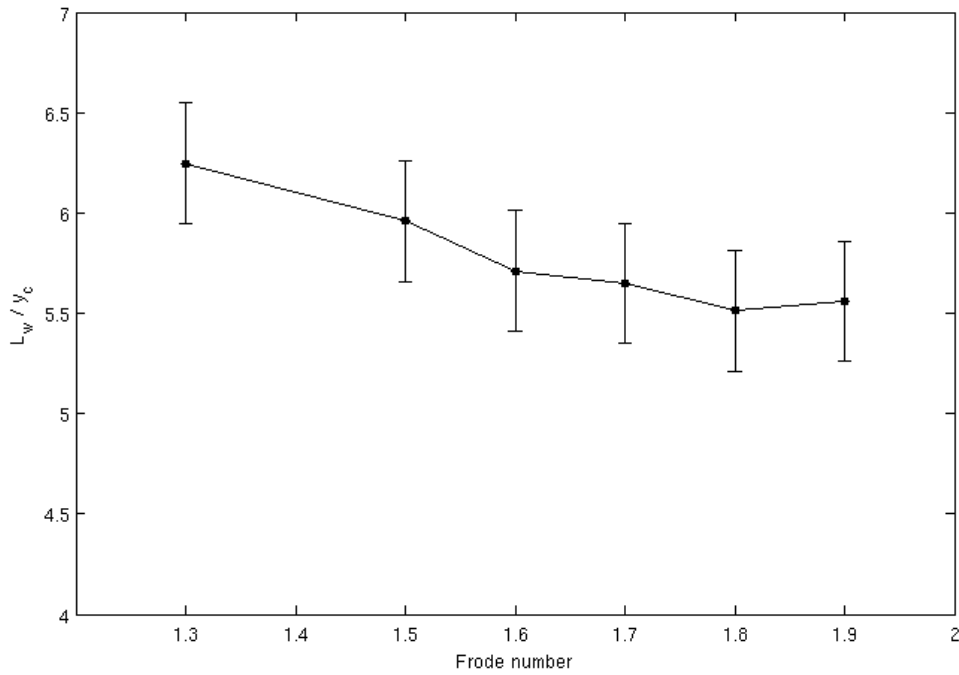


Fig 3-21: Dimensionless wave length from first to second crest. $N=7$ Res: $\delta_v=21$

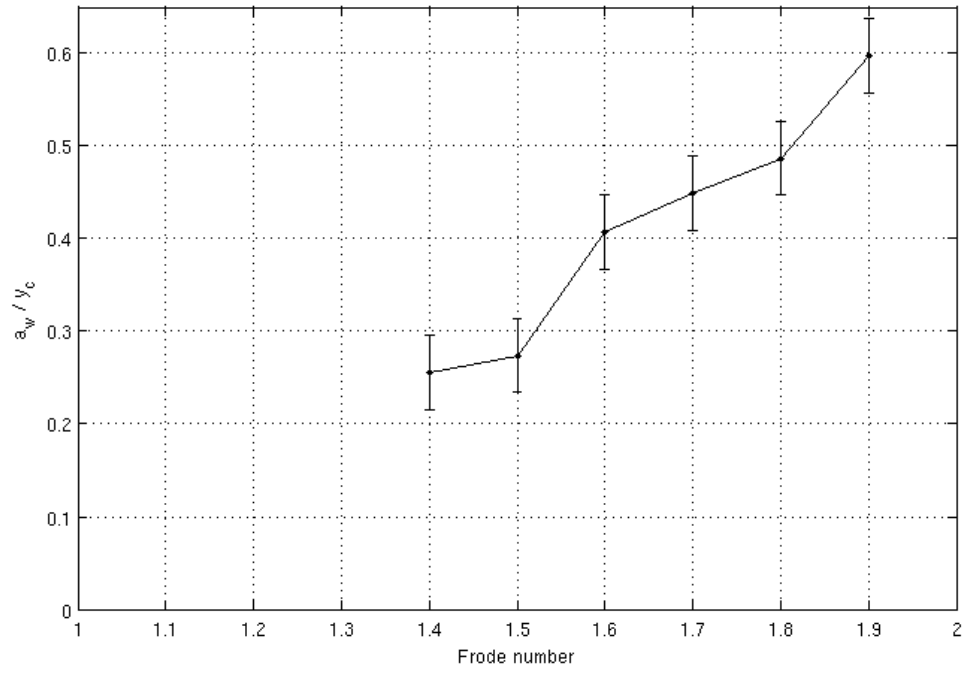


Fig 3-22: Dimensionless wave amplitude. $N=7$ Res = $\delta_v=21$

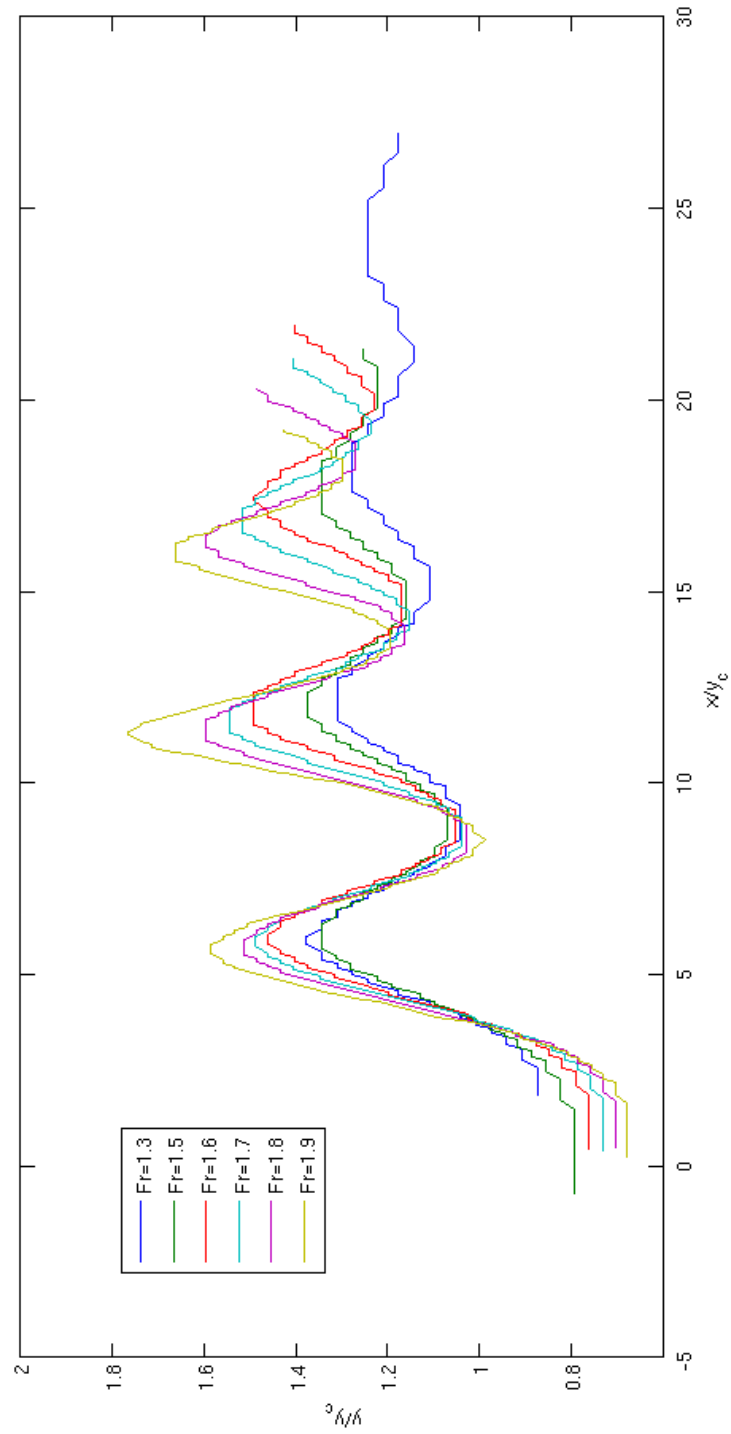


Fig 3-23: Free surface profiles for different Froude numbers.
Res: $\delta = 21$

3.4.4. Instability for critical waves

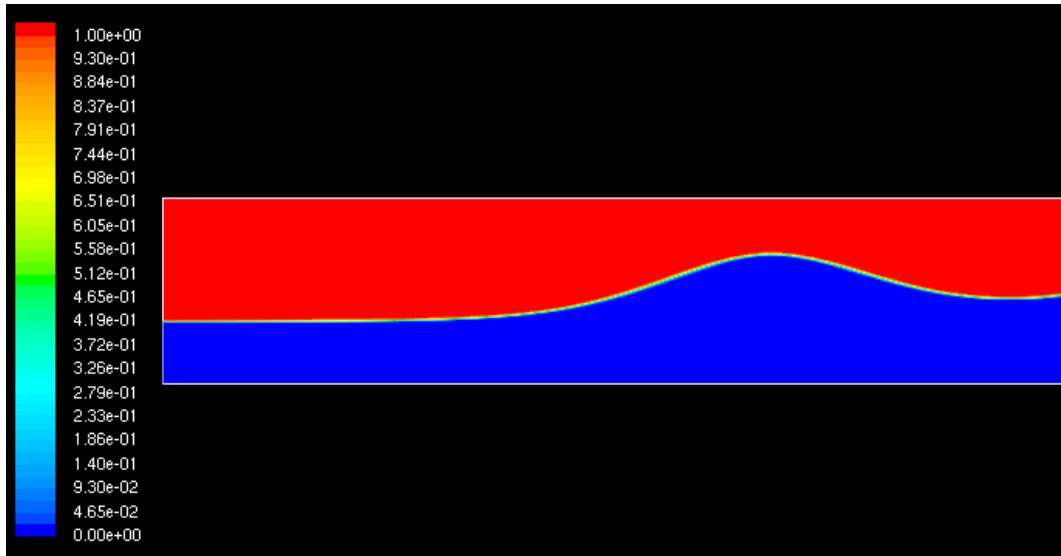


Fig 3-24: Phase field of a smooth undular jump for $N=10$, $\text{Res } \delta_v=34$

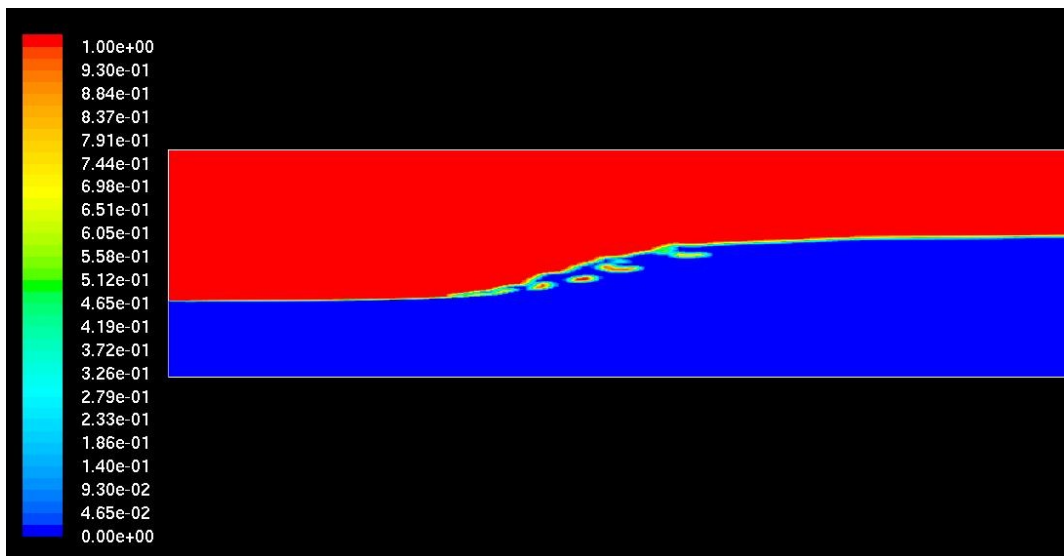


Fig 3-25: Phase field of a broken wave as alternate solution of Fig 3-24, $\text{Res } \delta_v=34$

Complex system and numerical simulation can sometimes show bifurcations. This means that different steady solutions can be found with slightly different initial conditions but same boundary conditions. During numerical simulations we observed that wave breaking sometime occurs and can be a steady alternate solution of a stable and smooth wave train (see Fig 3-24 and Fig 3-25). Wave breaking involve water flow turning upstream with formation of foam and air entrainment. The final steady state is basically a direct jump. However, foam can be not resolved properly by the grid and the simulation is not quantitatively realistic even is it look somehow similar to the real one. With some perturbation at the model, the alternate solution can be avoided if occurs and a stable wave train can be simulated. In all studies performed in this work we have always looked for the smooth steady state when possible. The instability is observed more often when the wave amplitude is great or we are close to the critical state.

In real waves, a similar instability can be observed when wave steepness reaches a critical value. Little modifications of the channel bed or discharge changes, can suddenly modify the appearance of the positive surge. Moreover, the turbulent perturbation of the flow could yields a sort of non-periodic cycle in which the wave brakes and become smooth again. The foam formed by the wave breaking, needs a good perturbation to be eliminated, this means that in low turbulence flow, like artificial channel, if foam is formed, is harder to see such cycle. Our numerical model can't simulate this cycle because no velocity inlet perturbation are involved, but when critical conditions occur, the instability of the numerical solution is an index of this bifurcation.

4. Conclusions

4.1. Undular jump

4.1.1. General considerations

The model, applied to the undular jump, shows reliable results and thus is able to simulate such class of near critical flow phenomena. The comparison with the experimental data (Chanson 2005) demonstrates the scale invariance and the validity of a two dimensional approach. Scale invariance in the turbulent range is well known in fluid dynamic and allows us to make numerical studies without relate them to the scale. Using the critical depth as length scale, the results of the simulations can be superimpose with the experiment data with a scale factor of 2.5. The two dimensional approach verifies that undular jump is a proper two dimensional phenomenon and that the lateral boundary effects in real channels are not responsible of the undular jump formation. The good results of the simulations also demonstrate that hydraulic momentum balance equations Eq.(1-15) can be applied in the numerical model because boundary conditions have been defined following this equation.

Outlet conditions are in general a critical issue in the simulation of a subcritical flow. Upstream propagation of numerical error or strong influence of the outflow boundary could be found. Moreover, in steady solution reverse flow of the gas phase must occurs in the upper part of this boundary to balance the outflow carried by the surface friction with liquid phase. Considering all these numerical critical issues, pressure outlet, with open channel options, worked well in all simulations and we haven't found any problem. To decrease computation cost, we also placed the boundary in a wavy region (about 3 wavelength from the first crest) and a specific test showed the small influence of this choice.

The sensitivity analysis over the parameters of the model, as the grid resolution or the placement of the outflow boundary, yield that the simulations are sensible to any little modification but the differences are confined in an acceptable range of accuracy. This kind of sensitivity on physical parameters of the inflow boundary have also been studied. Small changes of the turbulent intensity and velocity curvature profile yield small differences in numerical results. This behavior is consistent with real channel because any small difference in boundary conditions yield modification of the flow. In example, waves in natural rivers with constant discharge, can slightly change during the time because of small modification of the river bed due to erosion or deposition of material.

4.1.2. Necessary parametrized models

In Fluent, in order to simulate all fundamental fluid dynamic physics processes, we need to use few parametrized model in addition to the general fluid equations:

- Standard $k-\epsilon$ turbulence model
- Wall functions
- Geometric interface reconstruction

These models, with the standard fluid equations, yield reliable results comparable with

experimental data.

4.1.3. Sensitivity

Waves created by the undular jump can be described using the wave length, wave amplitude, velocity field, turbulent fields etc... These characteristics depend on the boundary conditions, in specific, the velocity inlet and the pressure outlet. During this work and using as reference the standard channel (see 3.1.6.), we have found two dependencies from the inlet conditions summarized below.

- The velocity profile curvature has a relevant task in the organization of the flow in the downstream waves. We found that large vertical shear yields an easier organization in order to have a smooth undular jump. In reverse, an almost constant velocity profile tends to form a direct jump or waves near the critical threshold.
- Turbulent energy supplied at the inflow, tends to break the organization of the velocity. This yields that high turbulent energy increase the wave amplitude and a critical threshold has been found.

These considerations show how the formations of the undular jump is related to the organization of the inflow. Strong vertical shear, associated here with an high degree of organization, make wave formation easier. Turbulence instead tends to decrease the degree of organization and thus make the wave formation harder. Natural rivers present in general strong vertical shears due to the high friction with the irregular bed. This could be the reason why waves occur frequently in high roughness river bed.

4.1.4. Essential physical conditions

Few boundary conditions are necessary to simulate an undular jump in a horizontal channel with an upstream Froude number of 1.6 :

- Velocity inlet profile has to be in the range defined by the threshold found in paragraph 3.4.1..
- Turbulence at the inlet has to be null or in the range defined in paragraph 3.4.2.
- Downstream free surface level must follows Eq.(1-15)

If this conditions are verified, we expect the undular jump formation. Experimental studies in wide channel should be performed to verify these conditions.

4.1.5. Wave characteristic, dependencies from Froude number

In the studies on the wave characteristic dependencies from the Froude number (see 3.4.3.) we have identify two clear behaviors increasing Froude number from 1.3 to the critical threshold 1.9:

- Wavelength slowly decreased
- Wave amplitude significantly increase with an almost linear relation

Since we believe that the dependency from inflow parameters can't be disregarded, we haven't defined any quantitative relations between wave characteristic and Froude number but we have identify two qualitative behaviors that we can expect for all inflow

conditions in the non critical ranges.

4.2. *Applicability of the model to open channel studies*

4.2.1. Applicability fields

Fluent model defined in paragraph 2.2. can be used to study open channel with near critical flows. The validation with the undular jump simulations has shown positive results and this tool is ready to be used for similar phenomena. However some restriction to the applicability field has to be done and, out of it, we can't guarantee the accuracy of the model. In this paper we have tested only the two dimensional version of Fluent and thus we can use the simulator only for channel in which the two dimensional approximation can be done. We can therefore study *wide channels* proprieties and predict velocity profiles, pressure field and flow depth even in complex two dimensional geometry. However we need to ensure that all the *length scales* can be resolved with enough discrete points by the model as described in paragraph 3.2.1.. With the tested resolutions, we have found good skill of the model in simulating the smooth wavy surfaces of the undular jump. The micro physics of the back flow, that we can associate at the foam, can't be simulated properly because has three dimensional feature and the length scale is much smaller than our grid resolution. This phenomenon occurs if the wave overtakes some critical parameters as the Froude number, the curvature of the inlet velocity profile or the turbulent intensity. However, we can still use the simulator to find critical parameters that define wave breaking because they are found through a series of reliable simulations. Over this critical parameters the simulations become quantitative unreliable even if they look qualitative correct.

4.2.2. Computation cost

All the models used in the simulator are strictly necessary to yield reliable results. Thus, no time can be saved simplifying the models. Unsteady VOF model may takes lot of time to reach the steady solution from an arbitrary initial condition. Thus, a way to save calculation time is to impose initial condition as close as possible to the expected steady solution. However, the parameter that affects more the calculation time is the grid resolution. With a standard 3 GHz CPU the calculation time may differs from a day for $\delta_v=34$, to several weeks for $\delta=85$. As we have seen in paragraph 3.2.1., the increment of the resolution over a certain threshold, may not improve the quality of the results. Therefore, working with high resolution meshes could be expensive and does not yield any significant quality improvement. For two dimensional structured mesh and near critical flow simulations, we have defined that the lowest resolution that yields good results, is about 20 points for the smaller phenomenon length-scale. Another approach with Fluent that could save calculation time even if more elaborated, is to adapt the grid where necessary. Fluent can perform simulations in low resolution till the steady solution is found, and then perform a grid adaption in the high shear region and in the interface to improve the quality. This method could be really useful in three dimensional simulations in which calculation cost have to be taken in account. Moreover, in order to reach a good steady solution in less time, it's possible to run the model with a large time step (Courant number around unit) and, when steady solution is closer, to decrease the time step in order to simplify the convergence of the governing equations.

4.3. Future studies

4.3.1. Improving the model

Fluid dynamic for open channel flows has been historical studied with real experiment based on the scale invariance. This work is just a first step in the introduction of numerical simulators. The model need to be tested in the three dimensional version, more useful and with a wider applicability range even if the calculation cost is high. It's also necessary to study a model to parametrize foam behaviors in order to perform quantitative studies in presence of rolls and broken flow in general. The required resolution to resolve foam is probably an unacceptable request for a Fluent simulation of an open channel. Near critical flows in natural rivers and in artificial channel in fact, show often foam formation in presence of a non regular bed.

4.3.2. Possible applications

Using the defined model, this work presents few analysis of the critical parameters that characterize wave breaking. Future studies are still necessary to understand all the synergy between the inflow conditions and to define in a more general way the critical thresholds. For example, is interesting to understand how the velocity profile shape affect the wave breaking at different Froude number and how the turbulent parameters affect the free surface with different velocity profiles.

At the moment, the simulator give reliable results in a certain applicability range (see 4.2.1.). A possible research within this range, could be to study the critical parameters of waves created by a step of small amplitude placed between two subcritical flow regions (Fig 4-2 and Fig 4-3). The formation mechanism is similar to the undular jump but the velocity and pressure profiles are necessarily different because a vertical fall occurs before the first crest.

The final goal could be the simulations of channels with an high degree of complexity and near critical flow. These channels have been recently built in all over the world for recreational and sportive use (Fig 4-1). Complexity degree is high because three dimensional effects are involved and the presence of subcritical flow yields that the downstream conditions can affect the flow upstream. The presence of foam necessarily complicates the simulations. The introduction of numerical simulator in the design process could improve the quality of the results. With such tool, water structures could be predicted during design operations. At the moment the designers of these channels use experience and basic pattern already testes.



Fig 4-1: Artificial channel for sportive use in Spain in dry conditions. $15 \text{ m}^3/\text{s}$ of water are pumped at maximum discharge.



Fig 4-2: Undular jump formed by a drop in occasion of Tevere river flooding (Roma 2008)



Fig 4-3: Step undular jump in Naviglio channel (Turbigo, 2005)

Appendix A

From the momentum function equation (1-11) we have:

$$\beta_1 V_1^2 \frac{A_1}{g} + \frac{y_1^2}{2} b = \beta_2 V_2^2 \frac{A_2}{g} + \frac{y_2^2}{2} b$$

for the conservation of the discharge we can write

$$V_2 = \frac{A_1 V_1}{A_2}$$

and from the Froude number definition

$$V^2 = F^2 g y$$

with some little algebra we have

$$\left(2\beta_1 F_1^2 + 1\right) \frac{y_2}{y_1} = 2\beta_2 F_1^2 + \left(\frac{y_2}{y_1}\right)^3$$

$$(t)^3 - (2\beta_1 F_1^2 + 1)t + 2\beta_2 F_1^2 = 0 \quad t = \frac{y_2}{y_1}$$

this equation can be resolved in general but considering that for fairly straight prismatic channel β is not much different in the two channel sections, we can assume $\beta_1 = \beta_2 = \beta$. With these consideration we have two solutions

$$t' = 1$$

$$t'' = \frac{1}{2} \left(\sqrt{1 + 8\beta F_1^2} - 1 \right)$$

t' is the obvious solution in which the depth before and after the jump are the same and the flow is uniform. t'' define the relations between the initial depth and the sequent depth.

Appendix B

Here are presented the user define function for velocity inlet profile and for $k-\epsilon$ turbulent inlet profiles wrote in c++ language.

```
#include "udf.h"
#define N 7.0
#define VMED 2.28
#define YMAX 0.2
#define Puno 8.1
#define Pdue 7.7
#define YC 0.27
#define factor 1.0

DEFINE_PROFILE(x_velocity, thread, index)
{
    real x[ND_ND]; /* this will hold the position vector */
    real y;
    real ytemp;
    face_t f; /*number of face ID*/
    begin_f_loop(f, thread) /* loops over all faces in the thread passed
                               in the DEFINE macro argument */
```

```

    {
        F_CENTROID(x,f,thread);
        y = x[1];

        ytemp= pow(y/YMAX,(1/N));
        F_PROFILE(f,thread,index) = (VMED*(1/N+1))*ytemp ;
    }
end_f_loop(f,thread)
}

DEFINE_PROFILE(k_profile,thread,index)
{
    real x[ND_ND]; /* this will hold the position vector */
    real y;
    real Itemp;
    face_t f; /*number of face ID*/
    begin_f_loop(f,thread) /* loops over all faces in the thread passed
                            in the DEFINE macro argument */
    {
        F_CENTROID(x,f,thread);
        y = x[1];

        Itemp= pow( factor*((Puno- Pdue* y/YMAX) /100.0)*VMED,2.0);
        F_PROFILE(f,thread,index) = 3.0/2.0*Itemp;
    }
end_f_loop(f,thread)
}

DEFINE_PROFILE(e_profile,thread,index)
{
    real x[ND_ND]; /* this will hold the position vector */
    real y;
    real Itemp;
    face_t f; /*number of face ID*/
    begin_f_loop(f,thread) /* loops over all faces in the thread passed
                            in the DEFINE macro argument */
    {
        F_CENTROID(x,f,thread);
        y = x[1];

        Itemp= 3.0/2.0 * pow( factor*(Puno- Pdue* y/YMAX) /
100.0*VMED,2.0);
        F_PROFILE(f,thread,index) = pow(0.09,0.75)/ (0.07 *YC) *
pow(Itemp,0.75);
    }
end_f_loop(f,thread)
}

```

References

- [1] A. Treske, *Undular bores (favre-waves) in open channels – experimental studies*, J. Hyd. Res., IAHR 32 (3) (1994) 355–370. Discussion: 33 (3), 274–278.
- [2] A.F. Teles Da Silva, D.H. Peregrine, *Nonsteady computations of undular and breaking bores*, in: Proc. 22nd Int. Cong. Coastal Eng., vol. 1, ASCE Publ., Delft, The Netherlands, 1990, pp. 1019–1032.
- [3] A.J.C. Barré de Saint-Venant, *Théorie et Equations Générales du Mouvement Non Permanent des Eaux Courantes*, Comptes Rendus des séances de l'Académie des Sciences, Paris, France, Séance 17 July 1871, vol. 73, (1871), pp. 147–154 (in French).
- [4] F. Benet, J.A. Cunge, *Analysis of experiments on secondary undulations caused by surge waves in trapezoidal channels*, J. Hyd. Res., IAHR 9 (1) (1971) 11–33.
- [5] G.A. El, R.H.J. Grimshaw, A.M. Kamchatnov, *Evolution of solitary waves and undular bores in shallow-water flows over a gradual slope with bottom friction*, J. Fluid Mech. 585 (2007) 213–244.
- [6] J. Ponsy, M. Carbone, *Etude photogrammétrique d'intumescences dans le canal de l'Usine d'Oraison* (Basses-Alpes), J. Soc. Française de Photogram. 22 (1966) 18–28.
- [7] J. Sander, K. Hutter, *On the development of the theory of the solitary wave. A historical essay*, Acta Mech. 86 (1991) 111–152.
- [8] J.A. Cunge, *Undular bores and secondary waves – experiments and hybrid finite-volume modelling*, J. Hyd. Res., IAHR 41 (5) (2003) 557–558.
- [9] J.A. Sandover, P. Holmes, *The hydraulic jump in trapezoidal channels*, Water Power 14 (Nov. 1962) 445–449.
- [10] J.G. Caputo, Y. Stepanyants, *Bore formation, evolution and disintegration into solitons in shallow inhomogeneous channels*, Nonlinear Processes in Geophysics 10 (2003) 407–424.
- [11] O.C. Zienkiewicz, J.A. Sandover, *The undular Etude photogrammétrique d'intumescences dans le canal de l'Usine d'Oraison surge wave*, in: Proc. of the 7th IAHR Congress, vol. II, Lisbon, Portugal, paper D25, 1957, pp. D1–11.
- [12] P.A. Madsen, H.J. Simonsen, C.H. Pan, *Numerical simulation of tidal bores and hydraulic jumps*, Coastal Eng. 52 (5) (2005) 409–433.
- [13] P.A. Madsen, I.A. Svendsen, *Turbulent bores and hydraulic jumps*, J. Fluid Mech. 129 (1983) 1–25.
- [14] R.A.R. Tricker, *Bores, Breakers, Waves and Wakes*, American Elsevier Publ. Co., New York, USA, 1965.
- [15] R.H. Clarke, *The morning glory: an atmospheric hydraulic jump*, J. Appl. Meteorology 11 (1972) 304–311.
- [16] T.B. Benjamin, M.J. Lighthill, *On cnoidal waves and bores*, Proc. Roy. Soc. London Ser. A, Math. & Phys. Sci. 224 (1159) (1954) 448–460.
- [17] F. Serre, *Contribution à l'étude des écoulements permanents et variables dans les canaux*, J. La Houille Blanche (Dec. 1953) 830–872 (in French).
- [18] *Fluent 6.3 User guide*, September, 2006

- [19] G. K. Batchelor. *An Introduction to Fluid Dynamics*. Cambridge Univ. Press, Cambridge, England, 1967.
- [20] H. Chanson and T. Bratteberg (1997). *Experimental Investigations of Air Bubble Entrainment in Developing Shear Layers*. Report CH48/97, Dept. of Civil Engineering, University of Queensland, Australia, Oct., 309 pages
- [21] H. Chanson and T. Bratteberg (2000). *Experimental Study of the Air-Water Shear Flow in a Hydraulic Jump*. Intl JI of Multiphase Flow, Vol. 26, No. 4, pp. 583–607.
- [22] H. Chanson, *Current Knowledge In Hydraulic Jumps And Related Phenomena. A Survey of Experimental Results*, European Journal of Mechanics B/Fluids, Vol. 28, No. 2, pp. 191–210 (DOI: 10.1016/j.euromechflu.2008.06.004)
- [23] H. Chanson, *Flow characteristics of undular hydraulic jumps. Comparison with near-critical flows*, Report CH45/95, Dept. of Civil Engineering, University of Queensland, Australia, 1995, June, 202 p.
- [24] H. Chanson, *Physical modelling of the flow field in an undular tidal bore*, J. Hyd.Res., IAHR 43 (3) (2005) 234–244.
- [25] H. Favre, *Etude Théorique et Expérimentale des Ondes de Translation dans les Canaux Découverts*, Dunod, Paris, France, 1935 (in French).
- [26] H.P.G. Darcy, H.E. Bazin, *Recherches hydrauliques, Imprimerie Impériales, Paris, France, Parties 1ère et 2ème, 1865 (in French)*.
- [27] J. Boussinesq, *Memoires présentés par divers savants à l'Académie des sciences, Essai sur la theorie des eaux courantes* (Paris, 1877)
- [28] J.S. Montes, *A Study of the Undular Jump Profile*. Proc. 9th Australasian Fluid Mechanics Conference AFMC, Auckland, New Zealand, pp. 148–151 (1986)
- [29] J.S. Montes, *A study of the undular jump profile*, in: Proc. 9th Australasian Fluid Mechanics Conference AFMC, Auckland, New Zealand, 1986, pp. 148–151.
- [30] J.S. Montes, *Undular hydraulic jump – discussion*, J. Hyd. Div., ASCE 105 (HY9) (1979) 1208–1211.
- [31] J.V. Boussinesq, *Essai sur la Théorie des Eaux Courantes, Mémoires présentés par divers savants à l'Académie des Sciences*, Paris, France, vol. 23, Série 3 (1), supplément 24, 1877, pp. 1–680 (in French).
- [32] Paul Boss, *Computation of water surface with change of the flow type*, SpringerVerlang, (Berlin, 1919) pp 20 and 52
- [33] R. Lemoine, *Sur les ondes positives de translation dans les canaux et sur le ressaut ondulé de faible amplitude*, J. La Houille Blanche (March–April 1948) 183–185 (in French)
- [34] T.B. Benjamin, M.J. Lighthill, *On cnoidal waves and bores*, Proc. Roy. Soc. London Ser. A, Math. & Phys. Sci. 224 (1159) (1954) 448–460.
- [35] V. T. Chow, *Open-Channel Hydraulics* (McGraw-Hill, New York, 1959).